JOURNAL OF GEOPHYSICAL RESEARCH, VOL. 105, NO. D4, PAGES 4699–4718, FEBRUARY 27, 2000

# Parameterization of the scattering and absorption properties of individual ice crystals

Ping Yang[1] and K. N. Liou
Department of Atmospheric Sciences, University of California, Los Angeles

Klaus Wyser[2]
Department of Meteorology, Stockholm University, Stockholm

David Mitchell
Atmospheric Sciences Center, Desert Research Institute, Reno, Nevada

**Abstract.** We present parameterizations of the single-scattering properties for individual ice crystals of various habits based on the results computed from the accurate light scattering calculations. The projected area, volume, and single-scattering properties of ice crystals with various shapes and sizes are computed for 56 narrow spectral bands covering 0.2-5 $\mu$m. The ice crystal habits considered in this study are hexagonal plates, solid and hollow columns, planar and spatial bullet rosettes, and aggregates that are commonly observed in cirrus clouds. Using the observational relationships between the aspect ratios and the sizes of ice crystals, we can define the three-dimensional structure of these ice crystal habits with respect to their maximum dimensions for light scattering calculations. The volume and projected area of ice crystals, expressed in terms of the diameters of the corresponding equivalent spheres, are first parameterized by employing the ice crystal maximum dimensions. Further, various analytical expressions as functions of the effective dimensions of ice crystals have been developed to parameterize the extinction and absorption efficiencies, asymmetry factor, and the truncation of the forward peak energy in the phase function. The present parameterization scheme provides an efficient approach to obtain the basic scattering and absorption properties of nonspherical ice crystals.

## 1. Introduction

Cirrus clouds are globally distributed, being present at all latitudes. These clouds strongly influence weather and climate processes on all scales through their effects on the radiative budget of the Earth and atmosphere system. Recent satellite observations reveal that the global cirrus cover can be as high as 30-40% [*Wylie et al.*, 1994]. Increases of the high cloud cover have also been reported at a number of urban airports in the United States based on surface observations spanning 40 years [*Liou et al.*, 1990; *Frankel et al.*, 1997]. Ubiquitous cirrus clouds have been identified as one of the most uncertain components in regulating the Earth's climate and its variability [*Liou*, 1986, 1992; *Stephens et al.*, 1990].

Cirrus clouds are almost exclusively composed of nonspherical ice crystals with various shapes and sizes. Development of a reliable parameterization of the radiative properties of cirrus clouds for use in general circulation models (GCMs) and climate models requires the fundamental scattering and absorption properties of ice particles. The exact solution for light scattering by nonspherical ice crystals is not feasible because proper coordinate systems cannot be defined to solve the basic electromagnetic wave equations derived from Maxwell's equations. However, the ray-tracing technique based on the principles of geometric optics has been widely used to determine the single-scattering properties of ice crystals [*Cai and Liou*, 1982; *Takano and Liou*, 1989a; *Macke*, 1993; *Hess and Wiegner*, 1994].

On the basis of single-scattering parameters of ice particles computed from the conventional ray-tracing technique developed by *Takano and Liou* [1989a], pa-

[1]Now at Science Systems and Applications, Inc., Lanham, Maryland.

[2]Now at Institute for Computational Earth System Science, University of California, Santa Barbara, California.



Paper number 1999JD900755.
0148-0227/00/1999JD900755$09.00

rameterization of the solar radiative properties of cirrus clouds has been conducted by *Ebert and Curry* [1992] and *Fu and Liou* [1993]. More recently, *Fu* [1996] has employed the single-scattering properties of ice crystals computed from an improved geometric optics method developed by *Yang and Liou* [1996b] in carrying out the solar radiative transfer parameterization for cirrus clouds. However, these parameterization efforts have assumed that cirrus clouds contain well-defined columns and plates. Recent observations based on airborne two-dimensional (2-D) optical probes and balloon-borne replicators [*Heymsfield and Platt*, 1984; *Krupp*, 1991; *Arnott et al.*, 1994; *Kinne et al.*, 1994; *Sassen et al.*, 1995; *Mitchell et al.*, 1996a, b] have shown that the majority of ice crystals in cirrus clouds are bullet rosettes, solid and hollow columns, plates, and aggregates with sizes ranging from 5 to about 1000 $\mu$m. Some ice crystals such as aggregates usually display rough surfaces because of coalescence and collision during the ice crystal growth process. The nature of rough surface has also been observed for evaporating single ice crystals and polycrystalline ice in the laboratory [*Cross*, 1968].

The scattering and absorption properties of complex ice crystals substantially differ from those of well-defined hexagonal columns and plates [*Takano and Liou*, 1995; *Iaquinta et al.*, 1995; *Macke et al.*, 1996; *Yang and Liou*, 1998; *Wyser and Yang*, 1998]. Employing the anomalous diffraction theory (ADT) to solve for the single-scattering properties of ice crystals, *Mitchell et al.* [1996b] have shown that model cirrus clouds composed of bullet rosettes and planar polycrystals reflect twice or more of the incident radiation in comparison with those composed of hexagonal plates and columns. Thus there is a necessity to account for more realistic ice crystal habits in parameterization of the radiative properties of cirrus clouds. The present study is intended to provide the required database in parameterization forms for the single-scattering properties of ice crystals with various shapes and sizes commonly observed in the atmosphere. In section 2, we describe the method for the computations of the scattering and absorption properties of ice crystals. In section 3, we present the physical and mathematical bases for the development of analytical parameterizations of the single-scattering properties of various ice crystal types with respect to their maximum dimensions. Comparisons between the parameterization and accurate results follow in section 4. Finally, conclusions are given in section 5.

## 2. Scattering and Absorption Properties of Ice Crystals

The fundamental parameters that drive a radiative transfer program involving clouds are the extinction coefficient, single-scattering albedo, and phase function. In the delta two-stream/Eddington radiative transfer schemes widely used by climate modelers, the phase function is replaced by the asymmetry factor $g$. In the more accurate delta four-stream scheme, the first four coefficients of the Legendre expansion of phase function are used to specify the angular distribution of the scattered energy [*Liou et al.*, 1988]. The phase function for ice particles in the solar wavelengths usually displays a sharp forward peak produced by diffraction and the delta transmission [*Takano and Liou*, 1989a]. In order to improve the accuracy in radiative transfer calculations in two- and four-stream approximations, the strong forward peak in the phase function is accounted for via the delta function adjustment in the asymmetry factor, extinction coefficients, and single-scattering albedo on the basis of the similarity principle [*Liou*, 1992]. As a good approximation, the first four Legendre polynomial expansion coefficients of the truncated phase function can be expressed in terms of the adjusted asymmetry factor [*Fu and Liou*, 1993]. In this study, we focus on parameterizations of the extinction and absorption efficiencies, asymmetry factor, and the truncation of the delta transmission and diffraction peak without dealing with the details of the corresponding phase function.

Computation of the asymmetry factor that requires angular integration of the phase function is based on an improved geometric ray-tracing computational method, referred to as GOM2. In this method, the ray-tracing technique is used to solve the total electric and magnetic fields on the particle surface (near field) in which the complete phase interference configuration is accounted for. The near field is then mapped to the far field on the basis of the electromagnetic equivalence principle. The asymmetry factor determined from GOM2 converges to the exact result computed from the finite difference time-domain (FDTD) technique [*Yang and Liou*, 1996a] for size parameters on the order of 15-20. When size parameters are larger than about 100, the asymmetry factor computed from GOM2 is exactly the same as the one computed from the conventional ray-tracing technique [*Takano and Liou*, 1989a]. The ray-by-ray/Monte Carlo integration algorithm, a simplification of GOM2 [*Yang and Liou*, 1997], is used to compute the extinction and absorption cross sections for more complex ice crystal geometries such as hollow columns, bullet rosettes, and aggregates.

The present single-scattering calculations are carried out at the centers of the following ice crystal bin sizes: 3–5, 5–10, 10–20, 20–30, 30–40, 40–50, 50–70, 70–90, 90–110, 110–150, 150–200, 200–250, 250–300, 300–400, 400–500, 500–600, 600–700, 700–800, 800–1000, 1000-1300, 1300–1500, 1500–2000, 2000–3000, and 3000–4000 $\mu$m. These bin sizes are specified in terms of the maximum dimensions of ice crystals. Six ice crystal shapes commonly observed in cirrus clouds are considered in this study: plates, solid and hollow columns, planar bullet rosettes composed of four branches, spatial bullet rosettes, and aggregates. The geometries for the hollow columns and planar rosettes have been defined by *Takano and Liou* [1995]. The spatial bullet rosettes

are composed of multiple (randomly selected from two to six) bullet branches that are randomly oriented in space. An aggregate ice crystal is an arbitrary attachment of two to eight randomly selected hexagonal elements. The depth of the cavity structure for hollow columns is assumed to vary from 0 to $L/2$, where $L$ is the length of the c axis of the column.

To completely define the 3-D geometry for each ice crystal habit with a given maximum dimension in the light scattering computation, we have used the aspect ratio relationship derived from in situ observations, which have been presented in the literature. The aspect ratio for columns has been parameterized by *Mitchell and Arnott* [1994] on the basis of reanalysis of the observed data from ice crystal clouds presented by *Auer and Veal* [1970], which is given by

$$a = \begin{cases} 0.35L & L < 100\,\mu\text{m} \\ 3.48L^{0.5} & L \geq 100\,\mu\text{m} \end{cases}, \quad (1)$$

where the semiwidth and length of ice crsytals $a$ and $L$ are in microns. The aspect ratio relationships presented by *Auer and Veal* [1970] have been widely employed and validated in various studies concerning cirrus clouds [e.g., *Takano and Liou*, 1989b; *Ebert and Curry*, 1992; *Fu and Liou*, 1993; *Fu*, 1996; *Mitchell et al.*, 1996a, b; *Macke et al.*, 1996]. For columns with hollow structures observed in cirrus clouds, the cavity depth $d$ is assumed to vary randomly, given by

$$d = 2\xi\bar{d}, \quad (2)$$

where $\bar{d}$ is the mean cavity depth and $\xi$ is a random number uniformly distributed in (0,1). We assume $\bar{d}/L = 0.25$ in the present study.

For plates, we use the relationship of ice crystal semiwidth and length presented by *Pruppachar and Klett* [1980], given by

$$L = 2.4883a^{0.474} \qquad 5\,\mu\text{m} \leq a \leq 1500\,\mu\text{m}. \quad (3)$$

The preceding aspect ratio relationship is the same as that used by *Arnott et al.* [1994], except that the units in the present formulation are in microns.

For the bullet rosette shape, the aspect ratio is defined with respect to individual bullet branches. We use the result presented by *Mitchell and Arnott* [1994], which is derived by matching the size and projected-area relation obtained from in situ observations [*Arnott et al.*, 1994] as follows:

$$a = 1.1552L^{0.63}, \quad (4)$$

where $a$ and $L$ are the semiwidth and length of the hexagonal part of individual bullet elements. The pyramidal tip of a bullet element can be specified via the following relationship:

$$t = \sqrt{3}a/2\tan\alpha, \quad (5)$$

where $\alpha$ is the inclination angle with respect to the major axis of the bullet elements. We select $\alpha = 28°$ according to *Greenler* [1980].

The constructing procedure for aggregates has been presented by *Yang and Liou* [1998] using a relative unit in specifying ice crystal dimension. For a given maximum dimension of an aggregate, the coordinate values of particle apexes can be defined by rescaling the coordinate values so that the particle size is what is expected. For aggregates, the effect of rough surface is accounted for by using a two-dimensional Gaussian probability function [*Cox and Munk*, 1954]. The effect of surface roughness tends to smooth out the scattering peaks corresponding to halo features and to reduce the backscattering [*Yang and Liou*, 1998]. The single-scattering properties are presented under the condition that ice crystals are randomly oriented.

The solar spectrum covers from 0.2 to 5.0 $\mu$m and is divided into 56 bands. For each band, the refractive index of ice presented by *Warren* [1984] with a modification based on recent measurements [*Gosse et al.*, 1995] is averaged by using the solar spectral irradiance data from LOWTRAN7 [*Kneizys et al.*, 1988], given by

$$(\bar{m}_r, \bar{m}_i) = \int_{\lambda_1}^{\lambda_2} (m_r, m_i) S_\lambda d\lambda \Big/ \int_{\lambda_1}^{\lambda_2} S_\lambda d\lambda, \quad (6)$$

where $\lambda_1$ and $\lambda_2$ are the lower and upper wavelengths for the band, $S_\lambda$ is the solar irradiance spectrum, and $m_r$ and $m_i$ are the real and imaginary parts of the refractive index, respectively. Table 1 lists the lower and upper wavelengths, the mean refractive index, and the fraction of solar energy for the 56 bands, where $\Delta S$ and $S$ are defined as follows:

$$\Delta S = \int_{\lambda_1}^{\lambda_2} S_\lambda d\lambda, \quad (7)$$

$$S = \int_{0.2\mu\text{m}}^{5\mu\text{m}} S_\lambda d\lambda. \quad (8)$$

The wavelength at band-center, $\bar{\lambda}$, is used to determine the size parameter in the numerical computation. The ice particle projected area, the volume, and the single-scattering properties, including extinction and absorption efficiencies, asymmetry factor, phase function, and the delta transmission contribution, are computed for the aforementioned six ice crystal shapes.

## 3. Parameterization of the Scattering Properties for Individual Ice Crystals

In the single-scattering calculations, the ice crystal size for each type is specified by its maximum dimension, which defines the complete three-dimensional geometry through the assumed aspect ratio. The ice crystal volume $V$ and its projected area $A$ are parameters required in the parameterization of the single-scattering properties. To develop relationships between these two parameters and the maximum dimension, we define

**Table 1.** Optical Constants for the 56 Spectral Bands Used in the Present Single-Scattering Calculation

| band | $\lambda_1$, $\mu$m | $\lambda_2$, $\mu$m | $\bar{\lambda}$, $\mu$m | $\bar{m}_r$ | $\bar{m}_i$ | $\Delta S/S$ |
|---|---|---|---|---|---|---|
| 1 | 0.2000 | 0.2500 | 0.2250 | 1.36558 | 0.10807E-07 | 0.14617E-02 |
| 2 | 0.2500 | 0.3000 | 0.2750 | 1.33974 | 0.64647E-08 | 0.90338E-02 |
| 3 | 0.3000 | 0.4000 | 0.3500 | 1.32490 | 0.37273E-08 | 0.69212E-01 |
| 4 | 0.4000 | 0.4500 | 0.4250 | 1.31736 | 0.21684E-08 | 0.65395E-01 |
| 5 | 0.4500 | 0.5000 | 0.4750 | 1.31430 | 0.16664E-08 | 0.71633E-01 |
| 6 | 0.5000 | 0.6000 | 0.5500 | 1.31109 | 0.32391E-08 | 0.13594E+00 |
| 7 | 0.6000 | 0.7000 | 0.6500 | 1.30812 | 0.14590E-07 | 0.11631E+00 |
| 8 | 0.7000 | 0.8000 | 0.7500 | 1.30592 | 0.66370E-07 | 0.93110E-01 |
| 9 | 0.8000 | 0.9000 | 0.8500 | 1.30404 | 0.21768E-06 | 0.74322E-01 |
| 10 | 0.9000 | 1.0000 | 0.9500 | 1.30236 | 0.75725E-06 | 0.60990E-01 |
| 11 | 1.0000 | 1.1000 | 1.0500 | 1.30068 | 0.20042E-05 | 0.48843E-01 |
| 12 | 1.1000 | 1.2000 | 1.1500 | 1.29894 | 0.30927E-05 | 0.40250E-01 |
| 13 | 1.2000 | 1.3000 | 1.2500 | 1.29707 | 0.11750E-04 | 0.33726E-01 |
| 14 | 1.3000 | 1.4000 | 1.3500 | 1.29500 | 0.14468E-04 | 0.27711E-01 |
| 15 | 1.4000 | 1.5000 | 1.4500 | 1.29265 | 0.24479E-03 | 0.23428E-01 |
| 16 | 1.5000 | 1.6500 | 1.5750 | 1.28994 | 0.37300E-03 | 0.28713E-01 |
| 17 | 1.6500 | 1.8000 | 1.7250 | 1.28544 | 0.17852E-03 | 0.21715E-01 |
| 18 | 1.8000 | 1.9000 | 1.8500 | 1.28048 | 0.16530E-03 | 0.11259E-01 |
| 19 | 1.9000 | 1.9500 | 1.9250 | 1.27686 | 0.75179E-03 | 0.48834E-02 |
| 20 | 1.9500 | 2.0000 | 1.9750 | 1.27491 | 0.15221E-02 | 0.44660E-02 |
| 21 | 2.0000 | 2.1000 | 2.0500 | 1.27195 | 0.13330E-02 | 0.77588E-02 |
| 22 | 2.1000 | 2.2000 | 2.1500 | 1.26593 | 0.45603E-03 | 0.65217E-02 |
| 23 | 2.2000 | 2.3000 | 2.2500 | 1.25773 | 0.22590E-03 | 0.55430E-02 |
| 24 | 2.3000 | 2.4000 | 2.3500 | 1.24750 | 0.44220E-03 | 0.47098E-02 |
| 25 | 2.4000 | 2.6000 | 2.5000 | 1.22541 | 0.70542E-03 | 0.75414E-02 |
| 26 | 2.6000 | 2.7000 | 2.6500 | 1.18381 | 0.11651E-02 | 0.30448E-02 |
| 27 | 2.7000 | 2.8000 | 2.7500 | 1.12811 | 0.83089E-02 | 0.26532E-02 |
| 28 | 2.8000 | 2.8250 | 2.8125 | 1.07186 | 0.30001E-01 | 0.61121E-03 |
| 29 | 2.8250 | 2.8500 | 2.8375 | 1.04165 | 0.51022E-01 | 0.59123E-03 |
| 30 | 2.8500 | 2.8750 | 2.8625 | 1.00765 | 0.83365E-01 | 0.56927E-03 |
| 31 | 2.8750 | 2.9000 | 2.8875 | 0.97684 | 0.13707E+00 | 0.55316E-03 |
| 32 | 2.9000 | 2.9250 | 2.9125 | 0.96257 | 0.21109E+00 | 0.53611E-03 |
| 33 | 2.9250 | 2.9500 | 2.9375 | 0.97816 | 0.28361E+00 | 0.51860E-03 |
| 34 | 2.9500 | 2.9750 | 2.9625 | 1.00263 | 0.33756E+00 | 0.50344E-03 |
| 35 | 2.9750 | 3.0000 | 2.9875 | 1.02533 | 0.39525E+00 | 0.48723E-03 |
| 36 | 3.0000 | 3.0250 | 3.0125 | 1.06059 | 0.46646E+00 | 0.47233E-03 |
| 37 | 3.0250 | 3.0500 | 3.0375 | 1.12584 | 0.54515E+00 | 0.45419E-03 |
| 38 | 3.0500 | 3.0750 | 3.0625 | 1.24061 | 0.61158E+00 | 0.44344E-03 |
| 39 | 3.0750 | 3.1000 | 3.0875 | 1.37994 | 0.60673E+00 | 0.42987E-03 |
| 40 | 3.1000 | 3.1250 | 3.1125 | 1.48505 | 0.54676E+00 | 0.41635E-03 |
| 41 | 3.1250 | 3.1500 | 3.1375 | 1.55641 | 0.48354E+00 | 0.40516E-03 |
| 42 | 3.1500 | 3.1750 | 3.1625 | 1.61315 | 0.41231E+00 | 0.39206E-03 |
| 43 | 3.1750 | 3.2000 | 3.1875 | 1.64442 | 0.32627E+00 | 0.38170E-03 |
| 44 | 3.2000 | 3.2500 | 3.2250 | 1.63469 | 0.21929E+00 | 0.72946E-03 |
| 45 | 3.2500 | 3.3000 | 3.2750 | 1.59636 | 0.13127E+00 | 0.68518E-03 |
| 46 | 3.3000 | 3.4000 | 3.3500 | 1.53909 | 0.66519E-01 | 0.12596E-02 |
| 47 | 3.4000 | 3.5000 | 3.4500 | 1.47859 | 0.26777E-01 | 0.11280E-02 |
| 48 | 3.5000 | 3.6000 | 3.5500 | 1.43769 | 0.12467E-01 | 0.10122E-02 |
| 49 | 3.6000 | 3.7000 | 3.6500 | 1.41082 | 0.78744E-02 | 0.90806E-03 |
| 50 | 3.7000 | 3.8500 | 3.7750 | 1.38810 | 0.72135E-02 | 0.11927E-02 |
| 51 | 3.8500 | 4.0000 | 3.9250 | 1.36939 | 0.99840E-02 | 0.10318E-02 |
| 52 | 4.0000 | 4.2000 | 4.1000 | 1.35455 | 0.14579E-01 | 0.11628E-02 |
| 53 | 4.2000 | 4.4000 | 4.3000 | 1.34184 | 0.21615E-01 | 0.95537E-03 |
| 54 | 4.4000 | 4.6000 | 4.5000 | 1.34108 | 0.30005E-01 | 0.77271E-03 |
| 55 | 4.6000 | 4.8000 | 4.7000 | 1.34394 | 0.21139E-01 | 0.65793E-03 |
| 56 | 4.8000 | 5.0000 | 4.9000 | 1.33474 | 0.13938E-01 | 0.56607E-03 |

Read 0.10807E-07 as $0.10807\times10^{-7}$.

the spherical diameters with equivalent volume $D_v$ and equivalent projected area $D_a$ for nonspherical ice crystals as follows:

$$D_a = 2r_a = 2(A/\pi)^{1/2}, \tag{9}$$

$$D_v = 2r_v = (6V/\pi)^{1/3}, \tag{10}$$

where $r_a$ and $r_v$ are the radii of the equivalent-area and equivalent-volume spheres, respectively.

According to in situ observations, the aspect ratios of nonspherical ice crystals in cirrus clouds are related to their maximum dimensions for a specific ice crystal habit in a statistical manner. Thus we look for a parameterization of $D_a$ and $D_v$ in terms of the maximum dimension $D_{\max}$. On the basis of computed values of $D_a$ and $D_v$ versus $D_{\max}$ for each ice crystal shape, the following equations are developed to fit the data:

$$D_a = \exp[\sum_{n=0}^{4} a_n (\ln D_{\max})^n], \tag{11}$$

$$D_v = \exp[\sum_{n=0}^{4} b_n (\ln D_{\max})^n]. \tag{12}$$

The coefficients $a_n$ and $b_n$ are determined by a least squares fit in the logarithmic scale to the computed values for ($D_a$,$D_{\max}$) and ($D_v$,$D_{\max}$). Table 2 lists the coefficients $a_n$ and $b_n$ for the six ice crystal habits. Thus, by using (9)–(12), the projected area and volume of a nonspherical ice crystal can be obtained directly from the maximum dimension $D_{\max}$.

In the parameterization of the single-scattering properties of an ice crystal, we use a physical length defined by the ratio of volume to the projected area, $V/A$. It is approximately equal to the mean length of the ray paths inside a particle if the multiple internal reflections of rays are not accounted for, as in the case of ADT [*Bryant and Latimer*, 1969]. Thus the phase delay and absorption of the rays depend on $V/A$. From (4) and (5), we may define an effective diameter $d_e$ and an effective radius $r_e$ for a nonspherical ice crystal as follows:

$$d_e = 2r_e = D_v^3/D_a^2 = \frac{3}{2}V/A. \tag{13}$$

As will be illustrated later, $d_e$ is much smaller than $D_a$ and $D_v$ for a given maximum dimension $D_{\max}$. However, the $d_e$-$D_{\max}$ relationship varies with the ice crystal habit. For example, $d_e$ will differ for hollow and solid columns even if the two shapes have the identical maximum dimension and aspect ratio, because the volumes for the two are not the same.

The extinction efficiency for a sphere of radius $r$ can be approximated as follows [*van de Hulst*, 1957]:

$$Q'_{\text{ext}}(\beta,\rho) = 2 - 4\exp(-\rho\tan\beta)\left[\frac{\cos\beta}{\rho}\sin(\rho-\beta) + \left(\frac{\cos\beta}{\rho}\right)^2\cos(\rho-2\beta)\right] + 4\left(\frac{\cos\beta}{\rho}\right)^2\cos 2\beta, \tag{14}$$

where $\rho = 2\chi \mid m_r - 1 \mid$ is the phase delay that a ray undergoes after it passes through the center of the particle and $\chi = 2\pi r/\lambda$. The phase shift of the transmitted ray is given by $\beta = \tan^{-1}(m_i/(m_r - 1))$. If the diameter of a sphere is selected to be the effective dimension of a nonpsherical ice crystal (i.e., $d_e = 2r$), then the mean length of the ray paths is the same for nonspherical and spherical particles and (14) can be applied to determine the extinction efficiency as a function of ice crystal dimension. To incorporate the effect of nonsphericity of ice crystals, we first utilize the extinction efficiency ex-

**Table 2.** Fitting Coefficients for the Parameterization of the Diameters of the Equivalent Spheres With the Same Projected Area or Volume as Nonspherical Ice Crystals

Fitting Coefficients for Equivalent-Area Spherical Diameters

| | $a_0$ | $a_1$ | $a_2$ | $a_3$ | $a_4$ |
|---|---|---|---|---|---|
| Plate | 0.43773E+00 | 0.75497E+00 | 0.19033E-01 | 0.35191E-03 | -0.70782E-04 |
| Column | 0.33401E+00 | 0.36477E+00 | 0.30855E+00 | -0.55631E-01 | 0.30162E-02 |
| Hollow column | 0.33401E+00 | 0.36477E+00 | 0.30855E+00 | -0.55631E-01 | 0.30162E-02 |
| Bullet rosettes-4 | 0.15909E+00 | 0.84308E+00 | 0.70161E-02 | -0.11003E-02 | 0.45161E-04 |
| Bullet rosettes-6 | 0.14195E+00 | 0.84394E+00 | 0.72125E-02 | -0.11219E-02 | 0.45819E-04 |
| Aggregates | -0.47737E+00 | 0.10026E+01 | -0.10030E-02 | 0.15166E-03 | -0.78433E-05 |

Fitting Coefficients for Equivalent-Volume Spherical Diameters

| | $b_0$ | $b_1$ | $b_2$ | $b_3$ | $b_4$ |
|---|---|---|---|---|---|
| Plate | 0.31228E+00 | 0.80874E+00 | 0.29287E-02 | -0.44378E-03 | 0.23109E-04 |
| Column | 0.30581E+00 | 0.26252E+00 | 0.35458E+00 | -0.63202E-01 | 0.33755E-02 |
| Hollow column | 0.24568E+00 | 0.26202E+00 | 0.35479E+00 | -0.63236E-01 | 0.33773E-02 |
| Bullet rosettes-4 | -0.97940E-01 | 0.85683E+00 | 0.29483E-02 | -0.14341E-02 | 0.74627E-04 |
| Bullet rosettes-6 | -0.10318E+00 | 0.86290E+00 | 0.70665E-03 | -0.11055E-02 | 0.57906E-04 |
| Aggregates | -0.70160E+00 | 0.99215E+00 | 0.29322E-02 | -0.40492E-03 | 0.18841E-04 |

pression derived from ADT for a nonspherical ice crystal. Because the mean length for the ray paths inside an ice crystal, $l_m$, is approximately equal to $V/A$, the extinction efficiency for a nonspherical ice crystal can be expressed in the form

$$\begin{aligned} Q''_{\rm ext}(\rho_e,\beta,\alpha) &= 2\left[1-\exp\left(-\frac{2\pi}{\lambda}l_m m_i\right)\right. \\ &\quad \left.\times\cos\left(\frac{2\pi}{\lambda}l_m \mid m_r-1\mid +\alpha\right)\right] \\ &= 2\left[1-\exp\left(-\frac{2\pi}{\lambda}\frac{V}{A}m_i\right)\right. \\ &\quad \left.\times\cos\left(\frac{2\pi}{\lambda}\frac{V}{A}\mid m_r-1\mid +\alpha\right)\right] \\ &= 2\left[1-\exp\left(-\frac{2}{3}\rho_e\tan\beta\right)\cos\left(\frac{2}{3}\rho_e+\alpha\right)\right], \quad (15) \end{aligned}$$

where $\rho_e = 2\pi d_e \mid m_r - 1 \mid /\lambda$ is the effective phase delay. The parameter $\alpha$, which is not included in the conventional ADT formulation, is the mean constant phase shift for the ray transmission in nonspherical particles.

To account for the complex ray behavior associated with external reflection, two refractions, and multiple internal reflections inside an ice crystal, we have used a combination of (14) and (15) in the parameterization of the extinction efficiency for a given effective phase delay $\rho_e$ in the form

$$\begin{aligned} Q_{\rm ext}(D_{\max},m_r,m_i) &= (1-\xi)Q'_{\rm ext}(\beta_1,\eta_1\rho_e) \\ &\quad + \xi Q''_{\rm ext}(\beta_2,\eta_2\rho_e,\alpha), \quad (16) \end{aligned}$$

where the six coefficients $\beta_1$, $\beta_2$, $\eta_1$, $\eta_2$, $\alpha$, and $\xi$ can be determined by using the least squares fitting of the extinction efficiency computed from the light scattering code. A Monte Carlo searching technique described in the appendix is used to perform the nonlinear regression fitting. Table 3 lists the fitting coefficients in (16) for six ice crystal habits at seven representative wavelengths.

Similarly, to parameterize the absorption efficiency for nonspherical ice crystals, we use a combination of the approximate analytical expressions for equivalent spheres and for nonspherical ice crystals under the ADT assumption. The absorption efficiency for the equivalent sphere of diameter $d_e$ can be approximated as follows [*van de Hulst*, 1957]:

$$Q'_{\rm abs}(\gamma) = 1 + \frac{2\exp(-\gamma_e)}{\gamma_e} + \frac{2[\exp(-\gamma_e)-1]}{\gamma_e^2}, \quad (17)$$

where $\gamma_e = 4\chi_e m_i$ and $\chi_e = 2\pi r_e/\lambda$ is the effective size parameter of a nonspherical ice crystal. Equation (17) has a removable singularity at $\gamma_e = 0$. We use the Taylor expansion to remove this singularity when $\gamma_e \le 10^{-4}$. According to ADT, the absorption efficiency for a nonspherical ice crystal with the mean ray path length $V/A$ can be approximated as follows:

$$Q''_{\rm abs}(\gamma_e) = 1-\exp(-\frac{4\pi}{\lambda}m_i\frac{V}{A}) = 1-\exp(-\frac{2}{3}\gamma_e). \quad (18)$$

Both $Q'_{\rm abs}(\gamma_e)$ and $Q''_{\rm abs}(\gamma_e)$ approach 1 when $\gamma_e$ is very large, because the effect of external reflection that reduces the absorption efficiency is not accounted for in (17) and (18). To include the effect of external reflection in the parameterization, we develop the following expression:

$$\begin{aligned} Q_{\rm abs}(D_{\max},m_r,m_i) &= (1-\xi_1)[(1-\xi_2)Q'_{\rm abs}(\eta_1\gamma_e) \\ &\quad + \xi_2 Q''_{\rm abs}(\eta_2\gamma_e)], \quad (19) \end{aligned}$$

where the unknown coefficients $\xi_1$, $\xi_2$, $\eta_1$, and $\eta_2$ can be determined from the nonlinear least squares fitting regression technique. The parameter $\xi_1$ indicates the amount of energy associated with the external reflection and transmission. Table 4 lists the fitting coefficients in (19) for six ice crystal shapes at seven wavelengths.

After a number of numerical trial-and-error experiments, we find that the asymmetry factor for nonspherical ice crystals can be parameterized by using the following function with seven fitting parameters:

$$\begin{aligned} g(D,m_r,m_i) &= (1-\xi_7)f_1(\chi_e,\xi_1,\xi_2,\xi_3) \\ &\quad + \xi_7 f_2(\chi_e,\xi_4,\xi_5,\xi_6), \quad (20) \end{aligned}$$

where

$$\begin{aligned} f_1(\chi_e,\xi_1,\xi_2,\xi_3) &= (1-\xi_1) \\ &\quad \times\left\{1-\frac{1-\exp[-\xi_2(\chi_e+\xi_3)]}{\xi_2(\chi_e+\xi_3)}\right\}, \quad (21) \\ f_2(\chi_e,\xi_4,\xi_5,\xi_6) &= (1-\xi_4) \\ &\quad \times\{1-\exp[-\xi_5(\chi_e+\xi_6)]\}. \quad (22) \end{aligned}$$

The fitting parameters $\xi_1$–$\xi_7$ can be determined from nonlinear fitting of the values of the asymmetry factor computed from the light scattering program (Table 5).

As discussed by *Takano and Liou* [1989a], there is a delta function transmission through parallel ice crystal faces (e.g., a basal plane and opposite basal plane) at $\theta = 0°$ in conjunction with light scattering by polyhedral particles. The phase function that includes the contribution of the delta transmission can be expressed as follows:

$$P = 2f_\delta\delta(\cos\theta - 1) + (1-f_\delta)P'(\theta), \quad (23)$$

where $\theta$ is the scattering angle, $f_\delta$ is the contribution of the delta function to the total scattered energy, and $P'(\theta)$ is the normalized phase function excluding the delta transmission. Light scattered in the exact forward direction can be regarded as not being scattered at all [*van de Hulst*, 1980]. For this reason, the delta function should be removed and the corresponding single-scattering properties should be adjusted according to the similarity principle [*Takano and Liou*, 1989b; *Liou*, 1992].

Even after the removal of the delta transmission, $P'(\theta)$ normally displays a strong forward scattering peak caused by diffraction, as is evident from the phase function displayed in Figure 1 (right). In order to prop-

**Table 3.** Coefficients for Parameterization of the Extinction Efficiency for Six Ice Crystal Habits at Seven Spectral Bands

| band | $\eta_1$ | $\eta_2$ | $\beta_1$ | $\beta_2$ | $\alpha$ | $\xi$ |
|---|---|---|---|---|---|---|
| | | | *Plates* | | | |
| 6 | 0.41890E-01 | 0.40439E+01 | 0.22722E+00 | 0.31234E-01 | -0.40750E+01 | 0.82755E+00 |
| 14 | 0.10618E+01 | 0.52182E+00 | 0.97072E-01 | 0.47273E-01 | 0.76868E-03 | 0.14893E+00 |
| 23 | 0.12866E+01 | 0.50738E+00 | 0.39303E-01 | 0.19075E-01 | -0.21648E+01 | 0.13132E+00 |
| 27 | 0.14324E+01 | 0.74296E+00 | 0.14501E+00 | 0.20455E+00 | 0.21712E+00 | 0.42856E+00 |
| 36 | 0.14521E+01 | 0.10774E+00 | 0.14127E+01 | 0.13939E+01 | -0.59832E+01 | 0.72604E-01 |
| 50 | 0.98633E+00 | 0.53963E+00 | 0.21786E+00 | 0.59807E-01 | 0.29540E+01 | 0.20277E+00 |
| 54 | 0.12389E+01 | 0.50363E+00 | 0.16522E+00 | 0.58000E-01 | 0.29697E+01 | 0.77213E-01 |
| | | | *Columns* | | | |
| 6 | 0.25373E+01 | 0.21558E+00 | 0.97310E+00 | 0.20081E+00 | -0.98615E+00 | 0.27887E+00 |
| 14 | 0.16186E+00 | 0.25742E+01 | 0.79274E+00 | 0.56535E-01 | -0.85984E+00 | 0.99990E+00 |
| 23 | 0.10199E+01 | 0.28623E+01 | 0.16454E-03 | 0.43988E-01 | -0.57863E-05 | 0.15782E+00 |
| 27 | 0.17026E+00 | 0.14263E+01 | 0.89380E+00 | 0.27667E+00 | -0.37125E+00 | 0.96005E+00 |
| 36 | 0.80116E+00 | 0.43079E-01 | 0.14767E+01 | 0.14362E+01 | -0.31133E-04 | 0.34160E-01 |
| 50 | 0.11212E+01 | 0.13601E+01 | 0.21707E+00 | 0.93853E-01 | 0.19540E-01 | 0.38874E+00 |
| 54 | 0.38510E+00 | 0.13911E+01 | 0.67389E+00 | 0.19713E+00 | -0.11563E+00 | 0.88671E+00 |
| | | | *Hollow Columns* | | | |
| 6 | 0.24717E+00 | 0.25710E+00 | 0.11233E+01 | 0.10565E+00 | 0.52115E+01 | 0.69588E-01 |
| 14 | 0.11281E+01 | 0.45546E+00 | 0.13901E+01 | 0.37845E+00 | 0.37295E+01 | 0.51843E+00 |
| 23 | 0.71770E+00 | 0.18175E+01 | 0.93101E+00 | 0.10267E+00 | -0.11705E+01 | 0.34331E+00 |
| 27 | 0.27673E+00 | 0.17398E+01 | 0.67365E+00 | 0.28731E+00 | -0.52950E+00 | 0.72319E+00 |
| 36 | 0.48118E-01 | 0.22686E+01 | 0.14929E+01 | 0.12544E+01 | -0.91089E+00 | 0.85875E+00 |
| 50 | 0.39444E+00 | 0.84808E+01 | 0.11214E+01 | 0.26809E-01 | 0.56010E+01 | 0.44781E+00 |
| 54 | 0.34626E+00 | 0.46920E+01 | 0.76910E+00 | 0.13720E+00 | -0.28792E+01 | 0.53933E+00 |
| | | | *Planar Bullet Rosettes* | | | |
| 6 | 0.47601E+00 | 0.14059E+00 | 0.46345E+00 | 0.40848E+00 | 0.30208E+01 | 0.22249E+00 |
| 14 | 0.95264E+00 | 0.11236E+01 | 0.93517E-01 | 0.55081E-01 | 0.93615E+00 | 0.19110E+00 |
| 23 | 0.11237E+01 | 0.11941E+01 | 0.18702E+00 | 0.79970E-01 | -0.14583E-01 | 0.37520E+00 |
| 27 | 0.14226E+01 | 0.11788E+01 | 0.35542E+00 | 0.20492E+00 | 0.59164E+01 | 0.70319E+00 |
| 36 | 0.13495E+01 | 0.28093E-01 | 0.13953E+01 | 0.15075E+01 | -0.10435E+01 | 0.60294E-01 |
| 50 | 0.12417E+01 | 0.11926E+01 | 0.18009E+00 | 0.11047E+00 | -0.28203E-01 | 0.51154E+00 |
| 54 | 0.14225E+01 | 0.12125E+01 | 0.27511E+00 | 0.22896E+00 | -0.20770E+00 | 0.75244E+00 |
| | | | *Spatial Bullet Rosettes* | | | |
| 6 | 0.19639E+00 | 0.14100E+00 | 0.13262E+01 | 0.59117E+00 | 0.28365E+01 | 0.30732E+00 |
| 14 | 0.10060E+01 | 0.11566E+01 | 0.40929E+00 | 0.88402E-01 | -0.16874E+00 | 0.32115E+00 |
| 23 | 0.17752E+00 | 0.11748E+01 | 0.13237E+01 | 0.19574E+00 | 0.61616E+01 | 0.73168E+00 |
| 27 | 0.22439E+00 | 0.10798E+01 | 0.62315E+00 | 0.34127E+00 | 0.62296E+01 | 0.93440E+00 |
| 36 | 0.10521E+01 | 0.44727E-01 | 0.14357E+01 | 0.14705E+01 | -0.10941E+01 | 0.67347E-01 |
| 50 | 0.10495E+01 | 0.11576E+01 | 0.26206E+00 | 0.12201E+00 | -0.15485E+00 | 0.37465E+00 |
| 54 | 0.29168E+00 | 0.11604E+01 | 0.11522E+01 | 0.29101E+00 | -0.19831E+00 | 0.83287E+00 |

**Table 3.** (continued)

| band | $\eta_1$ | $\eta_2$ | $\beta_1$ | $\beta_2$ | $\alpha$ | $\xi$ |
|---|---|---|---|---|---|---|
| | | | *Aggregates* | | | |
| 6 | 0.16841E+01 | 0.80549E+00 | 0.19499E+00 | 0.31503E+00 | 0.17246E+01 | 0.31014E+00 |
| 14 | 0.12330E+01 | 0.92600E+00 | 0.10124E+00 | 0.41218E+00 | 0.59337E+01 | 0.45786E+00 |
| 23 | 0.15399E+01 | 0.11183E+01 | 0.78411E-02 | 0.31519E+00 | 0.59374E+01 | 0.79442E+00 |
| 27 | 0.99594E+00 | 0.67082E-01 | 0.26889E+00 | 0.76534E+00 | 0.26688E-02 | 0.34230E-01 |
| 36 | 0.12142E+01 | 0.13182E+00 | 0.14000E+01 | 0.13393E+01 | -0.11291E+01 | 0.10159E+00 |
| 50 | 0.13440E+01 | 0.10800E+01 | 0.84415E-01 | 0.31149E+00 | -0.26007E+00 | 0.67022E+00 |
| 54 | 0.99548E+00 | 0.22298E+01 | 0.21425E+00 | 0.15618E+00 | -0.68980E+00 | 0.94093E-01 |

The data for other wavelengths are available from P. Yang.

erly account for this peak in radiative transfer calculations, thousands of Legendre polynomial terms are required in the phase function expansion. *Takano and Liou* [1989b] have proposed an extrapolation scheme in which the forward peak is truncated by extrapolating the phase function from scattering angle 10° to 0° in the logarithmic scale. In the present study, the truncation of the forward scattered energy is carried out on the basis of the integrated distribution of scattered energy defined by

**Table 4.** Coefficients for Parameterization of the Absorption Efficiency for Six Ice Crystal Habits at Seven Spectral Bands

| Band | $\eta_1$ | $\eta_2$ | $\xi_1$ | $\xi_2$ |
|---|---|---|---|---|
| | | *Plates* | | |
| 6 | 0.14677E+00 | 0.19160E+01 | 0.35195E+00 | 0.99990E+00 |
| 14 | 0.47742E+02 | 0.65393E-02 | 0.14220E+00 | 0.95981E+00 |
| 23 | 0.94834E+01 | 0.26628E-01 | 0.22255E+00 | 0.77564E+00 |
| 27 | 0.27094E+01 | 0.47334E+00 | 0.16792E-02 | 0.55632E+00 |
| 36 | 0.14044E+01 | 0.57591E-01 | 0.23544E+00 | 0.37456E-01 |
| 50 | 0.48187E+01 | 0.35216E+00 | 0.16117E-01 | 0.59088E+00 |
| 54 | 0.49015E+00 | 0.28564E+01 | 0.53851E-01 | 0.61923E+00 |
| | | *Columns* | | |
| 6 | 0.27215E-01 | 0.23241E+01 | 0.25201E+00 | 0.90977E+00 |
| 14 | 0.10476E+02 | 0.12044E+00 | 0.79766E+00 | 0.18274E+00 |
| 23 | 0.30199E+01 | 0.53832E-01 | 0.36157E+00 | 0.15646E+00 |
| 27 | 0.93271E+00 | 0.19525E+01 | 0.28433E-01 | 0.36587E+00 |
| 36 | 0.13588E+00 | 0.11045E+01 | 0.23657E+00 | 0.93931E+00 |
| 50 | 0.19785E+01 | 0.39974E+00 | 0.67542E-01 | 0.53371E-01 |
| 54 | 0.23830E+01 | 0.12209E+01 | 0.69210E-01 | 0.46477E+00 |
| | | *Hollow Columns* | | |
| 6 | 0.15338E+00 | 0.16933E+01 | 0.69737E-01 | 0.96468E+00 |
| 14 | 0.17644E+02 | 0.13025E+00 | 0.87710E+00 | 0.18042E+00 |
| 23 | 0.37956E+01 | 0.96097E-02 | 0.42420E-01 | 0.54575E+00 |
| 27 | 0.47225E+00 | 0.18236E+01 | 0.59386E-01 | 0.64645E+00 |
| 36 | 0.11689E+01 | 0.89549E-01 | 0.22755E+00 | 0.89511E-01 |
| 50 | 0.28051E+00 | 0.23962E+01 | 0.85165E-01 | 0.79364E+00 |
| 54 | 0.18801E+01 | 0.13324E+00 | 0.86493E-01 | 0.47555E-01 |

**Table 4.** (continued)

| Band | $\eta_1$ | $\eta_2$ | $\xi_1$ | $\xi_2$ |
|---|---|---|---|---|
| | | *Planar Bullet Rosettes* | | |
| 6 | 0.70005E-01 | 0.20620E+01 | 0.17583E+00 | 0.88977E+00 |
| 14 | 0.21529E+01 | 0.82181E+01 | 0.80331E+00 | 0.99990E+00 |
| 23 | 0.44207E+01 | 0.81683E+00 | 0.12229E+00 | 0.74298E+00 |
| 27 | 0.22718E+01 | 0.83837E+00 | 0.33559E-01 | 0.65592E+00 |
| 36 | 0.10761E+01 | 0.74902E+01 | 0.22731E+00 | 0.88964E-01 |
| 50 | 0.34286E+01 | 0.88794E+00 | 0.71067E-01 | 0.55932E+00 |
| 54 | 0.25886E+01 | 0.86089E+00 | 0.63585E-01 | 0.42314E+00 |
| | | *Spatial Bullet Rosettes* | | |
| 6 | 0.26821E-01 | 0.18551E+01 | 0.26124E-01 | 0.96730E+00 |
| 14 | 0.18964E+01 | 0.17429E+01 | 0.21235E-01 | 0.99128E+00 |
| 23 | 0.17673E+01 | 0.26111E+01 | 0.38069E+00 | 0.99990E+00 |
| 27 | 0.97388E+01 | 0.12102E+01 | 0.51606E-05 | 0.97168E+00 |
| 36 | 0.78596E+00 | 0.44995E+01 | 0.19630E+00 | 0.34904E+00 |
| 50 | 0.30318E+01 | 0.86922E+00 | 0.94429E-01 | 0.47765E+00 |
| 54 | 0.25339E+01 | 0.84822E+00 | 0.80553E-01 | 0.40557E+00 |
| | | *Aggregates* | | |
| 6 | 0.52692E-01 | 0.19355E+01 | 0.83602E-01 | 0.92048E+00 |
| 14 | 0.78907E+01 | 0.21663E+01 | 0.26855E+00 | 0.99990E+00 |
| 23 | 0.50082E+01 | 0.15435E+01 | 0.13130E+00 | 0.93947E+00 |
| 27 | 0.93893E+00 | 0.23266E+01 | 0.33039E-01 | 0.26597E+00 |
| 36 | 0.11653E+01 | 0.74693E-01 | 0.21857E+00 | 0.24773E-01 |
| 50 | 0.25572E+01 | 0.10176E+01 | 0.64032E-01 | 0.44448E+00 |
| 54 | 0.23634E+01 | 0.93883E+00 | 0.58390E-01 | 0.40609E+00 |

The data for other wavelengths are available from P. Yang.

$$E(\theta) = \frac{1}{2}\int_{\theta}^{\pi} P'(\theta')\sin\theta' d\theta', \tag{24}$$

where $E(\theta)$ is the percentage of energy scattered in the directions between $\theta$ and $\pi$ if the total scattered energy is scaled to unity. As evident from Figure 1, a substantial amount of energy is scattered in a small region around $\theta = 0°$. We truncate $E(\theta)$ by using the linear extrapolation in the logarithmic scale based on its values within 5°–10°. The truncated distribution of the scattered energy is denoted by $E'(\theta)$. For scattering angles larger than 10°, $E(\theta)$ and $E'(\theta)$ are identical. Thus the energy associated with the truncated forward peak is given by

$$f = E(0°) - E'(0°). \tag{25}$$

After removing the delta function and truncating the forward scattering peak, the normalized phase function is denoted by $P''(\theta)$, which is related to the original phase function in the form

$$P(\theta) \approx 2f_t\delta(\cos\theta - 1) + (1 - f_t)P''(\theta), \tag{26}$$

where

$$f_t = f + f_\delta - ff_\delta. \tag{27}$$

The asymmetry factor, extinction cross section, and single-scattering albedo associated with the truncated phase function $P''(\theta)$ are denoted as $g''$, $\sigma''_{\text{ext}}$, and $\omega''$. Following *Takano and Liou* [1995], they are given by

$$g'' = (g - f_t)/(1 - f_t), \tag{28}$$

$$\sigma''_{\text{ext}} = (1 - f_t\omega)\sigma_{\text{ext}}, \tag{29}$$

$$\omega'' = \frac{(1 - f_t)\omega}{1 - f_t\omega}. \tag{30}$$

The truncation factor $f_t$ is an important parameter for application of the single-scattering properties of ice

**Table 5.** Coefficients for Parameterization of the Asymmetry Factor for Six Ice Crystal Shapes at Seven Spectral Bands

| band | $\xi_1$ | $\xi_2$ | $\xi_3$ | $\xi_4$ | $\xi_5$ | $\xi_6$ | $\xi_7$ |
|---|---|---|---|---|---|---|---|
| | | | | *Plates* | | | |
| 6 | 0.20448E-02 | 0.20591E-02 | 0.57074E+00 | 0.32972E-06 | 0.12479E-01 | 0.83350E+02 | 0.90694E+00 |
| 14 | 0.30775E-02 | 0.16725E-02 | 0.40038E+02 | 0.36048E-01 | 0.17852E-01 | 0.50084E+02 | 0.99900E+00 |
| 23 | 0.38376E-01 | 0.25859E+01 | 0.43717E+03 | 0.23714E-07 | 0.25783E-01 | 0.53019E-06 | 0.38908E+00 |
| 27 | 0.80754E-03 | 0.33571E+00 | 0.15345E-04 | 0.61660E-06 | 0.50058E-01 | 0.39183E+02 | 0.63132E+00 |
| 36 | 0.95113E-02 | 0.13858E-02 | 0.18431E+00 | 0.11083E-04 | 0.23793E+00 | 0.52947E+01 | 0.92787E+00 |
| 50 | 0.98453E+00 | 0.38775E-02 | 0.18586E+02 | 0.22620E-01 | 0.42654E-01 | 0.16322E+02 | 0.99900E+00 |
| 54 | 0.15263E-01 | 0.22716E+00 | 0.13225E-03 | 0.26236E-04 | 0.44607E+00 | 0.20759E+01 | 0.55601E+00 |
| | | | | *Columns* | | | |
| 6 | 0.10721E+00 | 0.18620E+00 | 0.27382E+02 | 0.63931E-03 | 0.77836E-03 | 0.48804E+01 | 0.12803E+00 |
| 14 | 0.24557E+00 | 0.10382E-01 | 0.12685E+02 | 0.11847E-02 | 0.42495E+00 | 0.43118E+00 | 0.66856E+00 |
| 23 | 0.14654E+00 | 0.16857E-01 | 0.31366E+00 | 0.13266E-04 | 0.25498E+00 | 0.42437E+01 | 0.71566E+00 |
| 27 | 0.14981E-04 | 0.62729E-01 | 0.39962E-03 | 0.91440E-04 | 0.17593E+00 | 0.57904E+01 | 0.86346E+00 |
| 36 | 0.49418E-02 | 0.84225E-01 | 0.85745E+01 | 0.65096E-01 | 0.40683E+00 | 0.20448E+01 | 0.94673E+00 |
| 50 | 0.50310E-01 | 0.11201E+01 | 0.11946E+01 | 0.46344E-11 | 0.33479E-01 | 0.10408E-03 | 0.30328E+00 |
| 54 | 0.13541E-01 | 0.52753E-01 | 0.56897E-04 | 0.25078E-01 | 0.17928E+00 | 0.30424E+01 | 0.94938E+00 |
| | | | | *Hollow Columns* | | | |
| 6 | 0.15362E+00 | 0.13909E-02 | 0.19732E+02 | 0.40084E-03 | 0.34831E-01 | 0.65524E+02 | 0.78314E+00 |
| 14 | 0.25771E+00 | 0.76743E-02 | 0.18480E+01 | 0.23262E-05 | 0.32736E+00 | 0.18271E+01 | 0.75776E+00 |
| 23 | 0.13750E+00 | 0.15537E-01 | 0.15356E+02 | 0.36577E-03 | 0.22000E+00 | 0.47508E+01 | 0.75897E+00 |
| 27 | 0.19130E-01 | 0.14711E+00 | 0.67418E+01 | 0.23382E-05 | 0.22097E+00 | 0.43622E+01 | 0.75569E+00 |
| 36 | 0.79292E-05 | 0.63908E-06 | 0.29267E-01 | 0.28695E-03 | 0.31241E+00 | 0.31328E+01 | 0.93447E+00 |
| 50 | 0.13795E-03 | 0.14285E+00 | 0.11804E-01 | 0.44730E-01 | 0.69814E+00 | 0.16443E+01 | 0.57295E+00 |
| 54 | 0.35381E-06 | 0.79836E+00 | 0.13540E-03 | 0.47581E-01 | 0.15758E+00 | 0.57494E+01 | 0.66174E+00 |
| | | | | *Planar Bullet Rosettes* | | | |
| 6 | 0.12908E+00 | 0.45217E-01 | 0.14237E+03 | 0.15044E-01 | 0.18777E-01 | 0.78205E+01 | 0.67404E-01 |
| 14 | 0.20676E-08 | 0.40745E-01 | 0.30621E-01 | 0.13898E+00 | 0.79347E+00 | 0.72449E-04 | 0.78840E+00 |
| 23 | 0.22576E+00 | 0.57613E-01 | 0.68935E-02 | 0.59601E-03 | 0.44059E+00 | 0.27077E+01 | 0.69900E+00 |
| 27 | 0.38410E-05 | 0.27386E+00 | 0.15761E+02 | 0.30303E-08 | 0.25284E+00 | 0.75689E+00 | 0.34609E+00 |
| 36 | 0.67374E-06 | 0.10201E-05 | 0.19095E-06 | 0.90334E-06 | 0.44781E+00 | 0.22256E+01 | 0.93377E+00 |
| 50 | 0.37119E-01 | 0.13755E+00 | 0.20950E-02 | 0.14815E-06 | 0.14149E+01 | 0.40265E+00 | 0.53024E+00 |
| 54 | 0.94780E-02 | 0.94808E-05 | 0.47087E-01 | 0.28280E-02 | 0.18584E+00 | 0.34918E+01 | 0.96726E+00 |
| | | | | *Spatial Bullet Rosettes* | | | |
| 6 | 0.12204E+00 | 0.54639E-01 | 0.88668E+02 | 0.31560E-01 | 0.12300E-02 | 0.64531E-02 | 0.14475E-02 |
| 14 | 0.34070E+00 | 0.38056E-01 | 0.18301E-01 | 0.48322E-07 | 0.71173E+00 | 0.16197E+00 | 0.67979E+00 |
| 23 | 0.20778E+00 | 0.56144E-01 | 0.38977E+01 | 0.21007E-04 | 0.44792E+00 | 0.24215E+01 | 0.67033E+00 |
| 27 | 0.11018E-06 | 0.58455E-01 | 0.11393E-01 | 0.54108E-04 | 0.22956E+00 | 0.44495E+01 | 0.88437E+00 |
| 36 | 0.91172E-02 | 0.13461E-05 | 0.40429E-03 | 0.15615E-01 | 0.45336E+00 | 0.21195E+01 | 0.94785E+00 |
| 50 | 0.20721E-05 | 0.12851E+00 | 0.43046E-02 | 0.32693E-01 | 0.10365E+01 | 0.80371E+00 | 0.56170E+00 |
| 54 | 0.60619E-01 | 0.74500E+00 | 0.20457E-05 | 0.11574E-05 | 0.15047E+00 | 0.69187E+01 | 0.57799E+00 |

**Table 5.** (continued)

| band | $\xi_1$ | $\xi_2$ | $\xi_3$ | $\xi_4$ | $\xi_5$ | $\xi_6$ | $\xi_7$ |
|---|---|---|---|---|---|---|---|
| | | | *Aggregates* | | | | |
| 6 | 0.33805E-02 | 0.31191E-05 | 0.10606E+02 | 0.18188E+00 | 0.15148E+00 | 0.93335E+01 | 0.93536E+00 |
| 14 | 0.61361E-04 | 0.14126E-03 | 0.10521E+02 | 0.21453E-01 | 0.20498E+00 | 0.55550E+01 | 0.79130E+00 |
| 23 | 0.41785E-02 | 0.18545E-02 | 0.82296E+00 | 0.92042E-04 | 0.24680E+00 | 0.39430E+01 | 0.79729E+00 |
| 27 | 0.46220E-07 | 0.59054E-01 | 0.24970E-02 | 0.13939E-06 | 0.26515E+00 | 0.34563E+01 | 0.88729E+00 |
| 36 | 0.93254E-04 | 0.55612E-03 | 0.11635E-07 | 0.36143E-03 | 0.54779E+00 | 0.12691E+01 | 0.93566E+00 |
| 50 | 0.41085E-15 | 0.98745E-01 | 0.23277E-04 | 0.28609E-01 | 0.50735E+00 | 0.18204E+01 | 0.66143E+00 |
| 54 | 0.66910E-01 | 0.12452E+01 | 0.20527E-08 | 0.15266E-10 | 0.13277E+00 | 0.62675E+01 | 0.61842E+00 |

The data for other wavelengths are available from P. Yang.

crystals to radiative transfer calculations. We find that it can be parameterized with respect to the effective size parameter of an ice crystal using the following expression:

$$f_t = \begin{cases} 0 & \chi_e \le \chi_0 \\ (1-\xi_5) f_1(\chi_e, \xi_1, \xi_2, -\chi_0) & \\ \quad +\xi_5 f_2(\chi_e, \xi_3, \xi_4, -\chi_0) & \chi_e > \chi_0 \end{cases}, \quad (31)$$

where the functions $f_1$ and $f_2$ have been defined in (21) and (22), respectively. The fitting parameters $\xi_1$–$\xi_5$ and $\chi_0$ are determined from the least squares regression technique (Table 6).

## 4. Validation of the Parameterization Scheme

In the preceding section, various analytical expressions have been developed for the projected area, the volume, and the single-scattering properties of ice crystals as a function of the maximum dimension for six principal shapes in which the detailed aspect ratio relationships are implicitly included in defining the ice crystal geometry. In this section, we present comparisons of the results obtained from the "exact" light scattering program and the proceeding analytical parameterization equations for a visible band (0.5–0.6 $\mu$m with

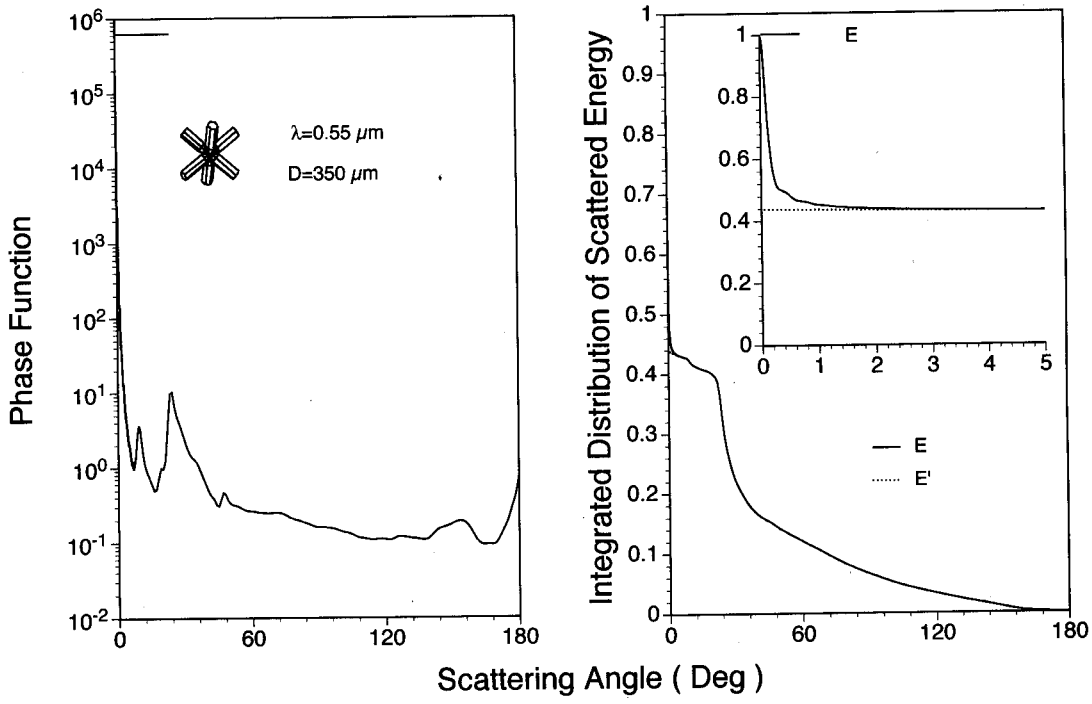


**Figure 1.** Phase function and the corresponding integrated distribution of the scattered energy for spatial bullet rosettes at a visible band. Also shown is the truncated integrated distribution of the scattered energy.

**Table 6.** Coefficients for Parameterization of the Truncation Factor for Six Ice Crystal Shapes at Seven Spectral Bands

| band | $\chi_0$ | $\xi_1$ | $\xi_2$ | $\xi_3$ | $\xi_4$ | $\xi_5$ |
|---|---|---|---|---|---|---|
| | | | *Plates* | | | |
| 6 | 0.00000E+00 | 0.23397E-02 | 0.19513E-02 | 0.51912E-04 | 0.15159E-01 | 0.81012E+00 |
| 14 | 0.13736E+02 | 0.39876E-02 | 0.44523E-02 | 0.23250E-04 | 0.29809E-01 | 0.83101E+00 |
| 23 | 0.13930E+02 | 0.89245E-02 | 0.34259E-02 | 0.14781E-02 | 0.36384E-01 | 0.89808E+00 |
| 27 | 0.11397E+02 | 0.57681E-01 | 0.58622E-02 | 0.10410E-01 | 0.44433E-01 | 0.93528E+00 |
| 36 | 0.14963E+02 | 0.96636E-07 | 0.21319E-01 | 0.66344E-08 | 0.24685E+00 | 0.66625E+00 |
| 50 | 0.11943E+02 | 0.12267E-04 | 0.28254E+01 | 0.69086E-01 | 0.51159E-01 | 0.92194E+00 |
| 54 | 0.12594E+02 | 0.24014E-01 | 0.15003E+00 | 0.14802E-06 | 0.66264E+00 | 0.19821E+00 |
| | | | *Columns* | | | |
| 6 | 0.00000E+00 | 0.60202E+00 | 0.85513E-03 | 0.97065E-01 | 0.21320E-01 | 0.66985E+00 |
| 14 | 0.12179E+02 | 0.68401E-04 | 0.32544E-01 | 0.59498E+00 | 0.43538E+00 | 0.52269E+00 |
| 23 | 0.14614E+02 | 0.33804E+00 | 0.34192E-01 | 0.14482E-04 | 0.55624E+00 | 0.22303E+00 |
| 27 | 0.11957E+02 | 0.55685E-03 | 0.98305E-01 | 0.11789E+00 | 0.11622E-01 | 0.29985E+00 |
| 36 | 0.10913E+02 | 0.12635E+00 | 0.38890E-02 | 0.19861E-01 | 0.53593E-01 | 0.80496E+00 |
| 50 | 0.14518E+02 | 0.71872E-01 | 0.46713E-01 | 0.13068E-02 | 0.16073E+00 | 0.32517E+00 |
| 54 | 0.17051E+02 | 0.15450E-03 | 0.38626E-01 | 0.88476E-01 | 0.17924E+00 | 0.63485E+00 |
| | | | *Hollow Columns* | | | |
| 6 | 0.00000E+00 | 0.13528E+00 | 0.34411E-01 | 0.43506E+00 | 0.27330E-01 | 0.99900E+00 |
| 14 | 0.10158E+02 | 0.77061E-04 | 0.63019E-01 | 0.68789E+00 | 0.49237E+00 | 0.60504E+00 |
| 23 | 0.12190E+02 | 0.26929E-01 | 0.59167E-01 | 0.63237E+00 | 0.46516E+00 | 0.58868E+00 |
| 27 | 0.99733E+01 | 0.53781E-01 | 0.20422E-01 | 0.53821E-02 | 0.78267E-01 | 0.44910E+00 |
| 36 | 0.91027E+01 | 0.17899E+00 | 0.49603E-02 | 0.17119E-01 | 0.62431E-01 | 0.80898E+00 |
| 50 | 0.12109E+02 | 0.18240E+00 | 0.49622E-01 | 0.31368E-05 | 0.16898E+00 | 0.36282E+00 |
| 54 | 0.14221E+02 | 0.17114E-03 | 0.17161E-01 | 0.11816E-02 | 0.18300E+00 | 0.64559E+00 |
| | | | *Planar Bullet Rosettes* | | | |
| 6 | 0.00000E+00 | 0.12534E-02 | 0.38929E-02 | 0.36593E+00 | 0.38827E-01 | 0.87616E+00 |
| 14 | 0.72313E+01 | 0.18693E-03 | 0.64995E-01 | 0.64049E+00 | 0.37112E+00 | 0.52616E+00 |
| 23 | 0.77252E+01 | 0.39255E+00 | 0.56464E-01 | 0.23050E-02 | 0.24497E+00 | 0.23801E+00 |
| 27 | 0.95882E+01 | 0.16832E-03 | 0.48881E-01 | 0.87794E-07 | 0.39396E+00 | 0.25270E+00 |
| 36 | 0.87512E+01 | 0.70136E-02 | 0.62228E-02 | 0.54136E-04 | 0.13341E+00 | 0.77993E+00 |
| 50 | 0.91081E+01 | 0.73364E-01 | 0.65102E-01 | 0.63820E-05 | 0.28242E+00 | 0.31428E+00 |
| 54 | 0.93186E+01 | 0.19090E-05 | 0.33232E-01 | 0.63333E-02 | 0.18539E+00 | 0.66460E+00 |
| | | | *Spatial Bullet Rosettes* | | | |
| 6 | 0.00000E+00 | 0.14875E+00 | 0.49514E-02 | 0.36201E+00 | 0.36993E-01 | 0.87020E+00 |
| 14 | 0.74435E+01 | 0.38449E-04 | 0.66128E-01 | 0.65184E+00 | 0.28135E+00 | 0.51997E+00 |
| 23 | 0.79430E+01 | 0.23964E-01 | 0.57470E-01 | 0.55293E+00 | 0.22208E+00 | 0.52053E+00 |
| 27 | 0.98386E+01 | 0.27812E-04 | 0.49104E-01 | 0.44721E-05 | 0.36379E+00 | 0.24827E+00 |
| 36 | 0.89798E+01 | 0.44982E-01 | 0.63790E-02 | 0.19674E-05 | 0.12523E+00 | 0.78368E+00 |
| 50 | 0.93435E+01 | 0.60448E-01 | 0.57105E-01 | 0.67976E-06 | 0.26961E+00 | 0.32363E+00 |
| 54 | 0.95557E+01 | 0.62343E-02 | 0.60737E-01 | 0.69327E-01 | 0.18888E+00 | 0.62995E+00 |

**Table 6.** (continued)

| band | $\chi_0$ | $\xi_1$ | $\xi_2$ | $\xi_3$ | $\xi_4$ | $\xi_5$ |
|---|---|---|---|---|---|---|
| | | | *Aggregates* | | | |
| 6 | 0.00000E+00 | 0.39026E-01 | 0.94264E-05 | 0.11281E-02 | 0.35218E-01 | 0.51453E+00 |
| 14 | 0.53891E+01 | 0.26238E-04 | 0.23014E-03 | 0.32951E+00 | 0.50467E-01 | 0.75998E+00 |
| 23 | 0.64672E+01 | 0.50450E-01 | 0.17705E-02 | 0.16208E+00 | 0.58463E-01 | 0.59619E+00 |
| 27 | 0.88675E+01 | 0.40901E-01 | 0.40653E-01 | 0.32697E-03 | 0.14787E+00 | 0.27522E+00 |
| 36 | 0.11288E+02 | 0.43800E-07 | 0.55831E-01 | 0.15613E+00 | 0.22976E+00 | 0.71040E+00 |
| 50 | 0.90091E+01 | 0.81093E-01 | 0.47913E-01 | 0.83114E-04 | 0.14362E+00 | 0.32312E+00 |
| 54 | 0.98007E+01 | 0.26431E-02 | 0.53431E-01 | 0.98604E-01 | 0.14625E+00 | 0.65814E+0 |

The data for other wavelengths are available from P. Yang.

a mean wavelength 0.55 $\mu$m) and a near-infrared band (3.7–3.85 $\mu$m with a mean wavelength 3.755 $\mu$m).

Figure 2 shows $D_a$, $D_v$, and $d_e$ as functions of $D_{\max}$. The data for $d_e$ are computed from the parameterization scheme based on (9)–(10) because only two of $D_a$, $D_v$, and $d_e$ are independent. An excellent agreement is shown between the parameterization results and the exact solutions derived from the 3-D ice crystal geometry. The overall feature illustrated in Figure 2 is that $D_a$ and $D_v$ are substantially larger than $d_e$, and $D_a$ is the largest among the three. *Yang and Liou* [1996a] have shown that using either equivalent-area or equivalent-volume spheres can significantly overestimate the scattering capacity of ice crystals. The $D_a$–$D_{\max}$, $D_v$–$D_{\max}$, and $d_e$–$D_{\max}$ relationships depend on the ice crystal geometry. For example, $d_e$ for hollow columns is smaller than that for solid columns.

The variations of $A$ and $V$ with respect to the maximum dimension $D_{\max}$ for various ice crystal shapes have been investigated by *Mitchell and Arnott* [1994] and *Mitchell et al.* [1996b]. These authors (MAM) have developed a number of parameterizations involving the projected area, volume, and an effective diameter in terms of the maximum dimension, principally based on

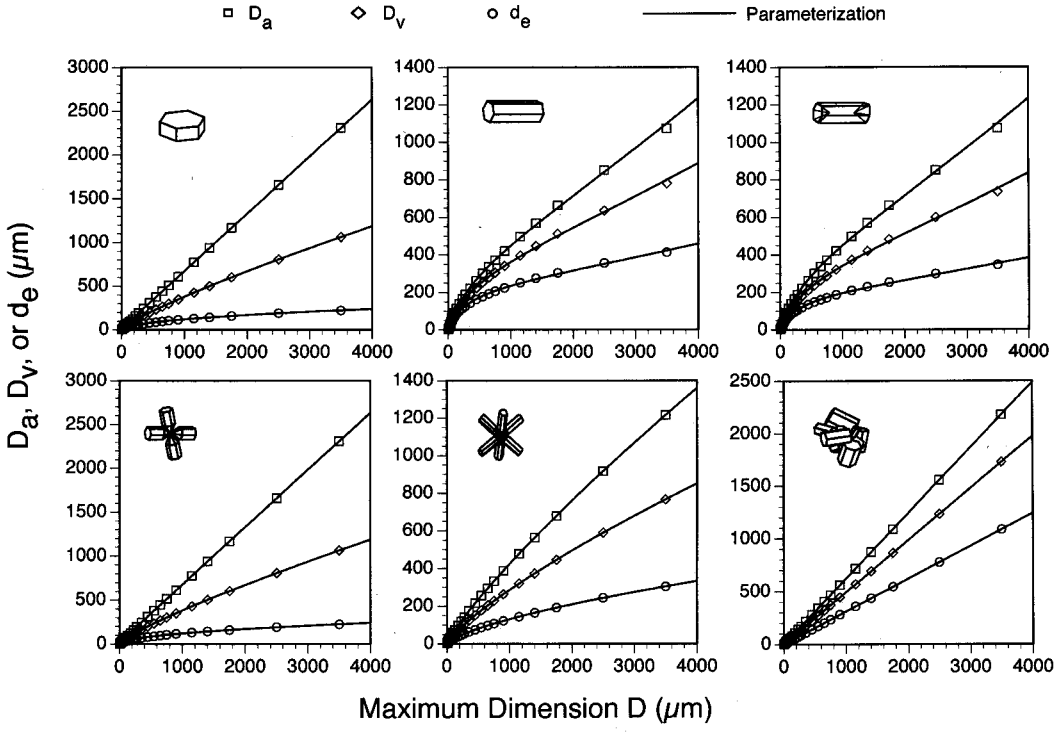


**Figure 2.** Comparisons of the $D_a$-$D_{\max}$, $D_v$-$D_{\max}$, and $d_e$-$D_{\max}$ relationships computed from the three-dimensional geometries of ice crystals and determined from the parameterization equations.

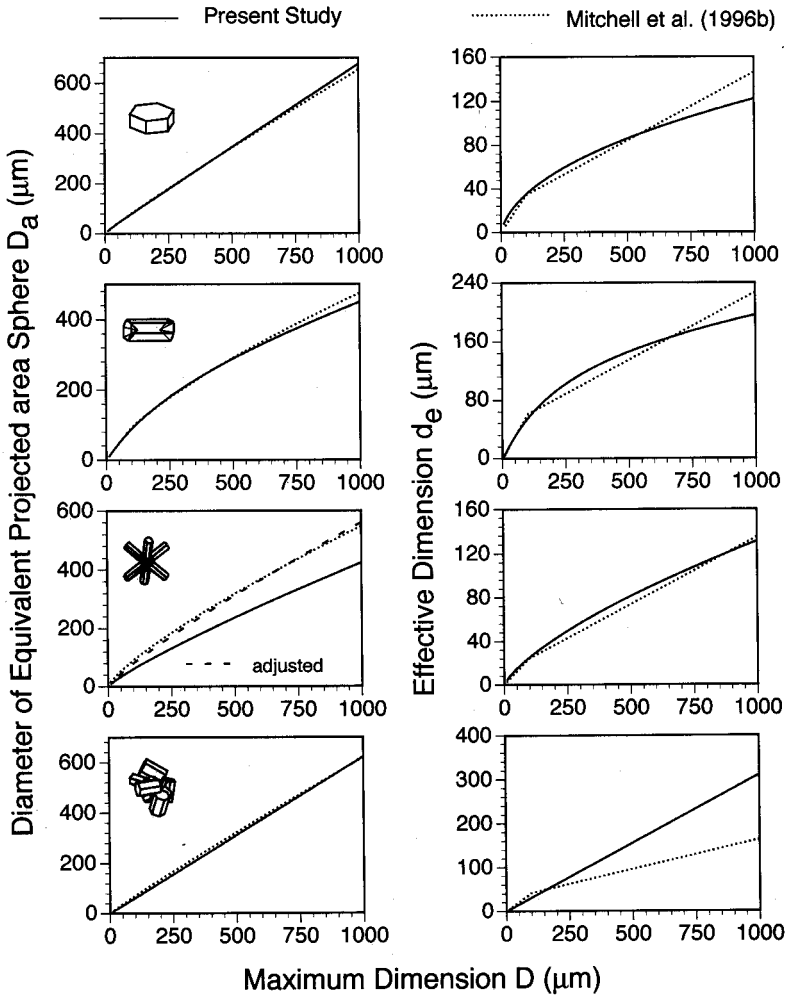


**Figure 3.** Comparisons of the $D_a$-$D_{\max}$ and $d_e$-$D_{\max}$ relationships based on the present parameterization equations and the results presented by [*Mitchell and Arnott* [1994] and *Mitchell et al.* [1996b].

available observations, in the forms

$$A = \sigma D_{\max}^{\delta}, \tag{32}$$

$$d_e^* = V/A = \gamma D_{\max} + \epsilon, \tag{33}$$

$$V = \rho_c 3\sqrt{3} W^2 D_{\max}/8\rho_0, \tag{34}$$

where $\sigma$ and $\delta$ are fitting coefficients depending on ice crystal habit; $\gamma$ and $\epsilon$ are regression values that are grouped according to $D_{\max}$ larger or smaller than 100 $\mu$m; and the volume expression is derived for columns only with the width $W$, the in situ mass density of a mixture of hollow and solid columns $\rho_c$, and the bulk ice density $\rho_0 = 0.92$ g/cm$^3$. Note that $3d_e^*/2 = d_e$. Figure 3 shows the $D_a$-$D_{\max}$ and $d_v$-$D_{\max}$ parameterization results from MAM and this study. For plates and columns, and the present parameterization results are almost identical to the MAM expressions in the $D_a$-$D_{\max}$ domain. However, substantial deviations are shown in the $d_e$-$D_{\max}$ domain when $D_{\max} > 125$ $\mu$m, because the later approach used a linear expression to parameterize $d_e$. For bullet rosettes, we use a random combination with two to six branches, while in MAM a five-branch model determined from 2D-C images is employed. Difference in the two approaches for $D_a$ amounts to a factor of 1.319. For the $d_e(= 3V/2A)$ case, the results are similar between the two because the effect of particle branch is canceled. For aggregates, the MAM studies utilize the replicator data for $D_{\max} < 200$ $\mu$m and 2D-C images for $D_{\max} > 200$ $\mu$m. The present parameterization matches closely with the measured results for the projected area case $D_a$. However, significant differences are noted for the $d_e$ results because MAM employ the hexagonal plates as surrogates in the computation of the volume of aggregates.

Figure 4 shows comparisons of the extinction efficiency obtained from the single-scattering program and the parameterization scheme. The oscillations of the extinction efficiency versus the effective phase delay $\rho_e$ for ray transmission are noted mainly for small size parameters, which are caused by the phase interferences of various localized waves. For large size parameters, the extinction efficiency essentially converges to 2. Substan-

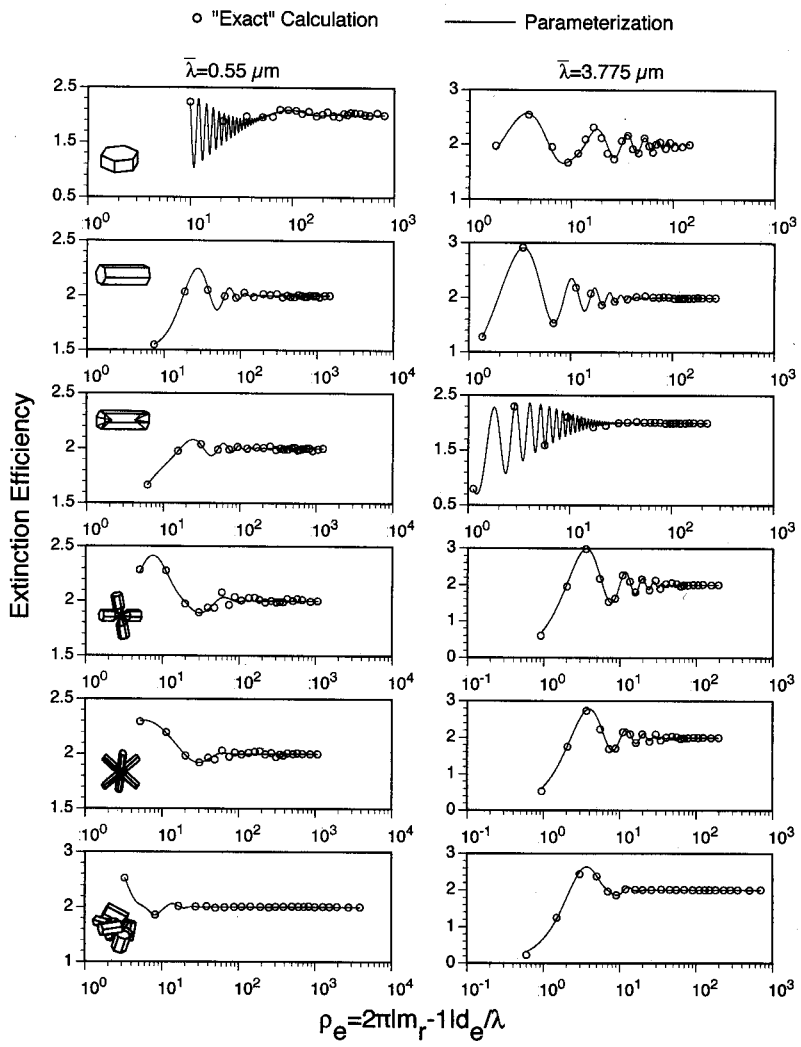


**Figure 4.** Comparisons of the extinction efficiency for six ice crystal shapes computed from the light scattering program and the parameterization for two wavelengths: 0.55 and 0.3775 $\mu$m.

tial dependence on the ice crystal shape is illustrated.

Figure 5 shows comparisons of the absorption efficiency as a function of the effective size parameter $\chi_e$. For the visible band, absorption by ice is extremely small, and the absorption efficiency increases with the ice crystal effective size parameter linearly. For the near-infrared band, absorption is saturated when the effective size parameter is larger than about 100. The difference between the saturated absorption efficiency and unity indicates the amount of the scattered energy associated with external reflections on the ice crystal surface, since the rays refracted into the ice crystal are essentially absorbed when saturated absorption is reached. From Figure 5, the scattered energy associated with external reflections is on the order of 5% of the total attenuated energy (scattered and absorbed energy), but the exact amount of the external reflection energy is dependent on ice crystal habit.

Shown in Figure 6 are comparisons of the asymmetry factor values computed by the light scattering program and parameterization equations. The contribution of the delta transmission is included in this illustration. For the visible band, the asymmetry factor is about 0.8 for all the ice crystal shapes except plate, which has a larger value. This is because a large amount of energy is scattered in the forward direction in conjunction with the delta transmission, leading to a strong forward peak. For the absorbing near-infrared band, the scattered energy is mainly produced by diffraction when size parameters are larger than about 100 with the asymmetry factor close to 1.

Figure 7 shows comparisons of the truncation factor $f_t$ defined in (27). At the visible band, the asymptotic value of $f_t$ is close to 0.5 for solid and hollow columns, bullet rosettes, and aggregates, because the truncated energy is the part associated with the diffraction peak. For the plate shape, truncation of the forward peak of the phase function includes both the delta transmission and the diffraction peak, which contain more than half of the total scattered energy. For the near-infrared band, the rays refracted into ice crystals are largely absorbed. As a result, the diffracted energy dominates the

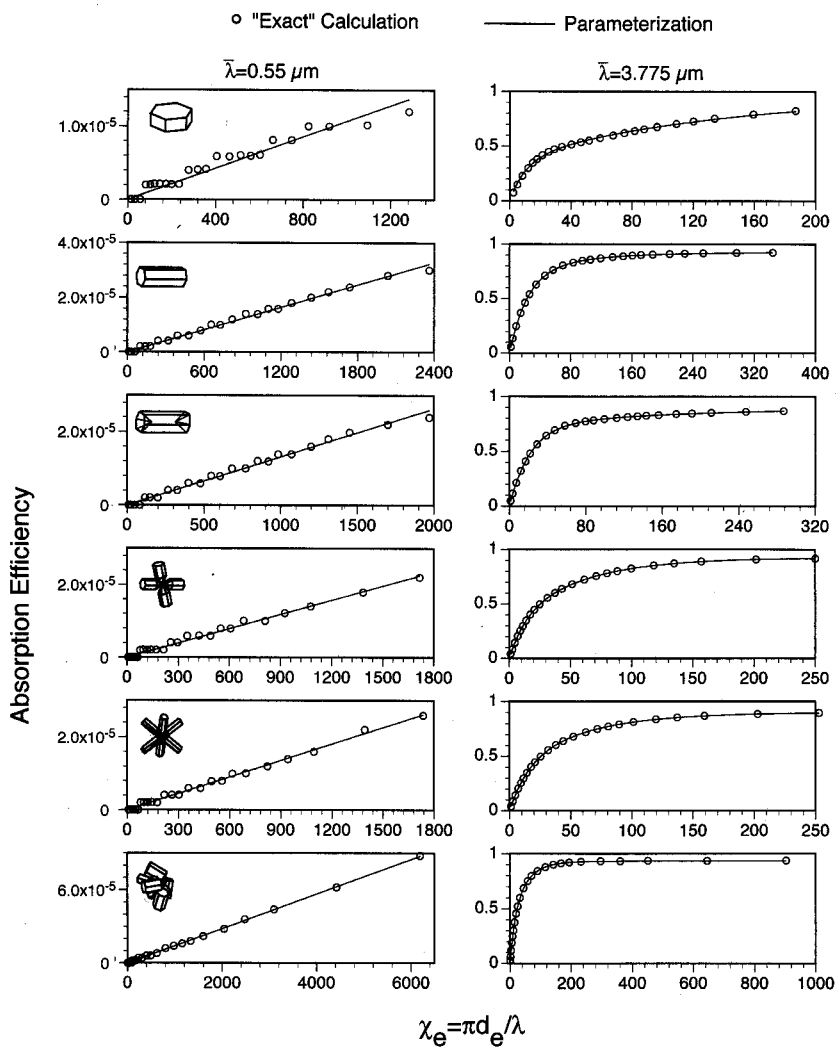


**Figure 5.** Same as Figure 4, except for the absorption efficiency.

total scattered energy. This is more significant for large particles, leading to a strong forward peak in the phase function with a truncation factor much larger than 0.5. The truncation factor is close to zero for small size parameters, because the delta transmission and strong forward diffraction do not occur owing to absorption and the effect of ray spreading [*Yang and Liou*, 1996b].

## 5. Conclusion

In this study, we have presented a parameterization of the single-scattering properties of six ice crystal types commonly occurring in cirrus clouds in terms of their maximum dimensions. We define the equivalent-volume and equivalent-projected-area spherical diameters ($D_v$ and $D_a$) of nonspherical ice crystals with respect to the maximum dimension. An effective dimension $d_e$, proportional to the mean ray path length within the ice crystal in the context of geometric ray tracing, is further defined in conjunction with the parameterization of the single-scattering properties for nonspherical ice crystals. The basic single-scattering properties for six ice crystal types are computed from an improved geometric optics method for the solar spectrum of 0.2–5 $\mu$m.

In the parameterization, $D_a$ and $D_v$ are first expressed in terms of the maximum dimension $D_{\max}$. Thus $d_e$ can be obtained analytically if $D_{\max}$ is specified. Furthermore, the extinction and absorption efficiencies, asymmetry factor, and the truncation factor associated with the removal of the strong forward diffraction peak and delta transmission in the phase function are parameterized as functions of $d_e$. The fitting coefficients in the parameterization equations are obtained from the nonlinear least squares regression calculations on the basis of a Monte Carlo researching technique. This parameterization allows an efficient calculation of the single-scattering properties of six ice crystal types once the the maximum dimensions are given, without carrying out the detailed and laborious light scattering calculations. To the extent that the assumed size-shape relationship applies to cirrus clouds, the present parameterization can be useful for the com-

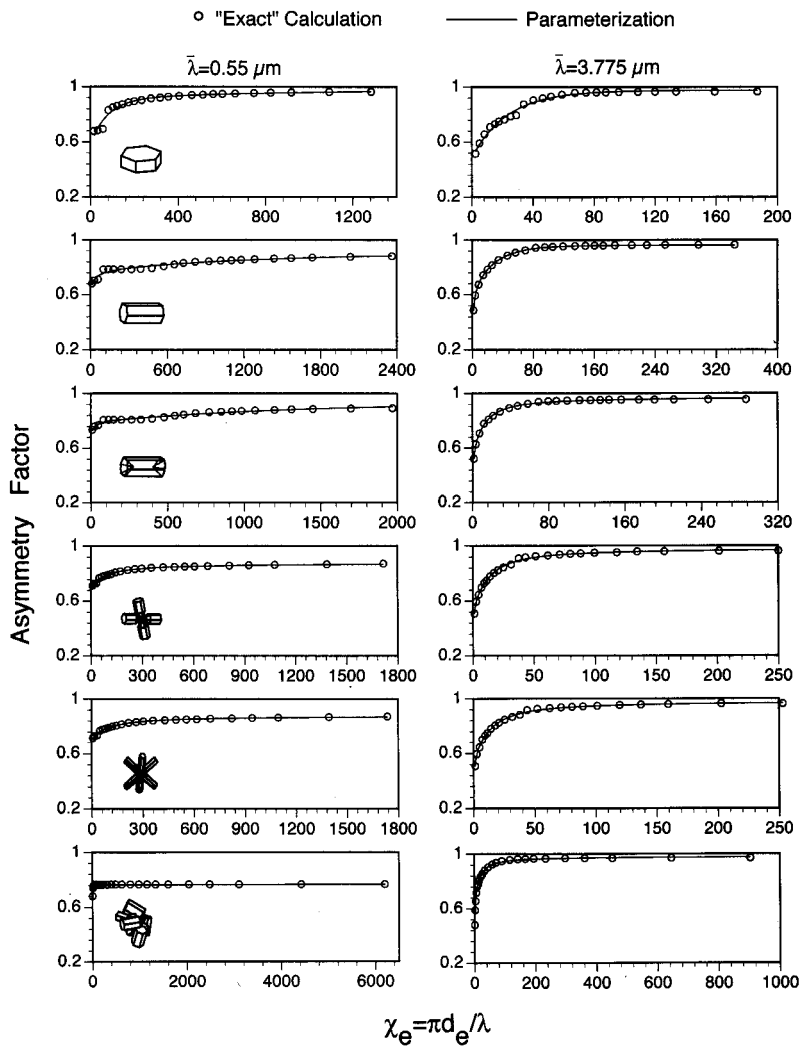


**Figure 6.** Same as Figure 4, except for the asymmetry factor without the truncation of the forward peak.

putation of the bulk solar radiative properties of cirrus clouds for applications to climate models.

## Appendix: Determination of the fitting coefficients in parameterization equations

Let $Y$ be one of the single-scattering properties computed from the light scattering program. We use nonlinear function $F(C_1, C_2, C_3, \ldots, C_n, x)$ to fit $Y$. In this function, $C_i$ are fitting coefficients, and $x$ is either the effective size parameters $\chi_e$ defined in (17), (20), and (31) or the effective phase delay $\rho_e$ defined in (16). The deviations between the single-scattering properties computed from the light scattering program and the parameterization equations are expressed by

$$\Delta = \sum_i [Y_i - F(C_1, C_2, C_3, \ldots, C_n, x)]^2, \qquad \text{(A1)}$$

where $Y_i$ is the values of $Y$ when $x = x_i$, and the summation is carried out for all the discrete ice crystal sizes at which the single-scattering computations are carried out. Under the least squares regression condition, the optimal fitting coefficient can be obtained via the following constraint condition:

$$\frac{\partial \Delta}{\partial C_i} = 0 \qquad i = 1, 2, 3, \ldots, n. \qquad \text{(A2)}$$

Equation (A2) leads to a set of nonlinear equations, which can be solved by numerical techniques such as the Newton-Raphson method. To avoid the complicity involved in the nonlinear equations, the Levenberg-Marquart linearization technique method [Press et al., 1986] can be applied to solve for the fitting coefficients. In this method, the deviation given in (A1) is expanded into a quadratic form and shooting of the optimal fitting coefficients is carried out on the basis of an iterative procedure.

In the aforementioned methods, initial guesses of the fitting coefficients must be provided in order to proceed with iterative calculations to achieve a convergent solution. This proves to be difficult for the nonlinear

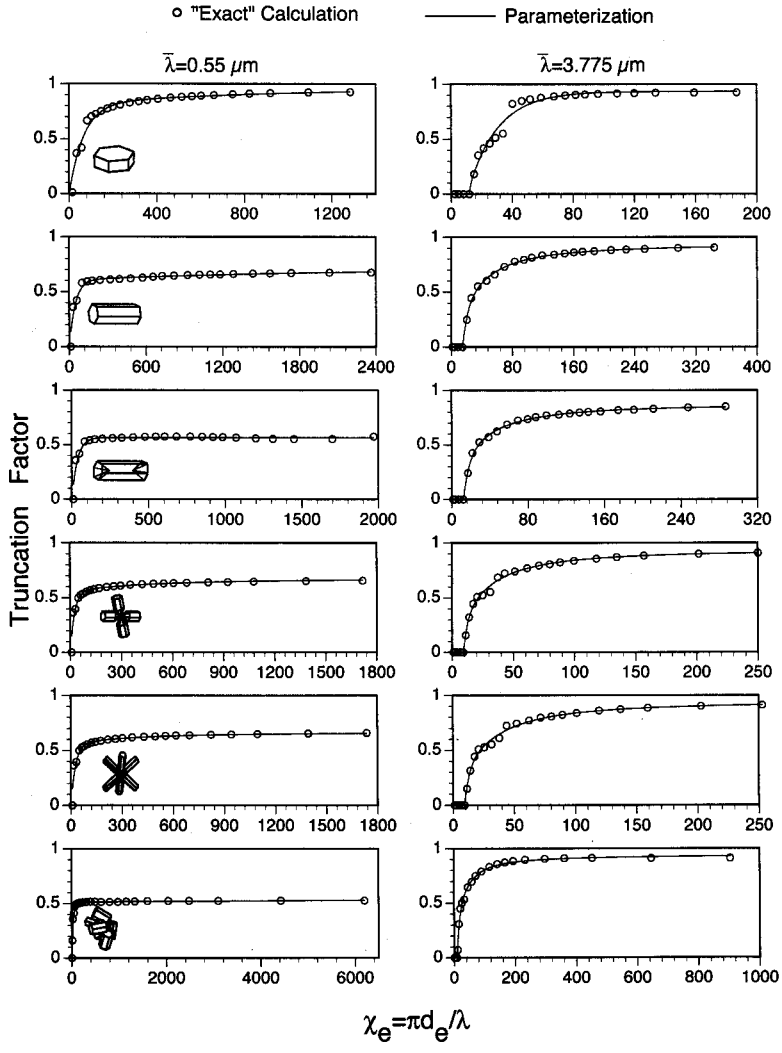


**Figure 7.** Same as Figure 4, except for the truncation factor (see text for the definition).

functions involved in this study, because the coefficient matrix may be ill-conditioned during the iterative calculations. To avoid these complications, we use a Monte Carlo searching technique to solve for the fitting coefficients. In this method, the possible variation range for $C_i$, $i = 1, \ldots, n$, is first determined. If $C_i$ belongs to the range $(C_{i,0}, C_{i,1})$, then we randomly select $C_i$ as follows:

$$C_i = C_{i,0} + R_i(C_{i,1} - C_{i,0}) \qquad i = 1, \ldots, n, \quad \text{(A3)}$$

where $R_i$ is a random number uniformly distributed in (0,1). We carry out $5 \times 10^7$ random sampling tests of the coefficients $C_i$ on the basis of (A3). The optimal coefficients are those that minimize the deviation given by (A1). To make the random sampling procedure efficient, we use the following algorithm: If $R_i$, $i = 1, \ldots, n$, are selected to determine the fitting coefficients on the basis of the Monte Carlo searching method for the first time sampling test, then the random numbers for the second time sampling test are given by $1 - R_i$, $i = 1, \ldots, n$; for the third time sampling test, $R_i$, $i = 1, \ldots, n$, are obtained from a random number generator again; for the fourth time sampling test, $1 - R_i$, $i = 1, \ldots, n$, is employed. This procedure is repeated until the $5 \times 10^7$ sampling tests are completed.

To improve the accuracy for the preceding method, a wide range of $(C_{i,0}, C_{i,1})$ is selected in the $5 \times 10^7$ sampling tests. We denote the optimal coefficients so obtained as $\tilde{C}_i$, $i = 1, \ldots, n$. Furthermore, another $5 \times 10^7$ random sampling tests are conducted to improve the accuracy on the basis of the following procedure. The fitting coefficient is evaluated via

$$C_i = 5R_i\tilde{C}_i \qquad i = 1, \ldots, n. \quad \text{(A4)}$$

Then, the deviation $\Delta$ is computed by using the sampled coefficients. If $\Delta$ decreases compared to the previous sampling test, $\tilde{C}_i$ is updated by $C_i$; otherwise, $\tilde{C}_i$ is left unchanged. We find that this procedure significantly improved the accuracy of fitting coefficients. To validate the Monte Carlo searching technique, this

method has been applied to a number of cases for which correct and convergent solutions can be efficiently obtained by using the Levenberg-Marquardt method. The relative differences between the results obtained by the two methods are less than 0.1%.

**Acknowledgments.** This study was supported by NSF grant ATM-93-1521, NASA grants NAG1-1719 and NAG5-2678, and DOE grant DE-FG03-95ER61991.

## References

Arnott, W. P., Y. Y. Dong, and J. Hallett, Role of small ice crystals in radiative properties of cirrus: A case study, FIRE II, November 22, 1991, *J. Geophys. Res., 99*, 1371-1381, 1994.

Auer, A. H., Jr., and D. L. Veal, The dimension of ice crystals in natural clouds, *J. Atmos. Sci., 27*, 919-926, 1970.

Bryant, F. D., and P. Latimer, Optical efficiencies of large particles of arbitrary shape and orientation, *J. Colloid Interface Sci., 30*, 291-304, 1969.

Cai, Q., and K. N. Liou, Polarized light scattering by hexagonal ice crystals: Theory, *Appl. Opt., 21*, 3569–3580, 1982.

Cox, C., and W. Munk, Measurement of the roughness of the sea surface from photographs of the Sun's glitter, *J. Opt. Am. Soc., 44*, 838-850, 1954.

Cross, J. D., Study of the surface of ice with a scanning electron microscope, in *Proceedings of International Symposium on Physics of Ice*, pp. 81–94, Plenum, New York, 1968.

Ebert, E. E., and J. A. Curry, A parameterization of ice cloud optical properties for climate models, *J. Geophys. Res., 97*, 3831–3836, 1992.

Frankel, D., K. N. Liou, S. C. Ou, D. P. Wylie, and P. Menzel, Observations of cirrus cloud extent and their impacts to climate, paper presented at the Ninth Conference on Atmospheric Radiation, Am. Meteorol. Soc., Long Beach, Calif., Feb. 2-7, 1997.

Fu, Q., An accurate parameterization of the solar radiative properties of cirrus clouds for climate models, *J. Clim., 9*, 2058-2082, 1996.

Fu, Q., and K. N. Liou, Parameterization of the radiative properties of cirrus clouds, *J. Atmos. Sci., 50*, 2008-2025, 1993.

Gosse, S., D. Labrie, and P. Chylek, Refractive index of ice in the 1.4 to 7.8 $\mu$m spectral range, *Appl. Opt., 34*, 6582-6586, 1995.

Greenler, R. G., *Rainbow, Halos, and Glories*, 195 pp., Cambridge Univ. Press, New York, 1980.

Hess, M., and M. Wiegner, COP: A data library of optical properties of hexagonal ice crystals, *Appl. Opt., 33*, 7740-7746, 1994.

Heymsfield, A. J., and C. M. R. Platt, A parameterization of the particle size spectrum of ice clouds in terms of the ambient temperature and the ice water content, *J. Atmos. Sci., 41*, 846-855, 1984.

Iaquinta, J., H. Isaka, and P. Personne, Scattering phase function of bullet rosette ice crystals, *J. Atmos. Sci., 52*, 1401-1413, 1995.

Kinne, S., R. Bergstrom, T. P. Ackerman, A. J. Heymsfield, J. Deluisi, M. Shiobara, P. Pilewskie, F. P. J. Valero, and Y. Takano, Cirrus cloud solar radiative properties: Comparisons between theory and observation based measurements during FIRE'91, paper presented at the Eighth Conference on Atmospheric Radiation, Am. Meteorol. Soc., Nashville, Tenn., Jan. 23-28, 1994.

Kneizys, F. X., E. P. Shettle, L. W. Abreu, J. H. Chetwynd, and G. P. Anderson, Users guide to LOWTRAN7, *Environ. Res. Pap. 1010*, 160 pp., Air Force Geophys. Lab., Hanscom Air Force Base, Mass., 1988.

Krupp, C., Holographic measurements of ice crystals in cirrus clouds during the International Cirrus Experiment ICE 1989, report of the Fourth Workshop at the Metorological Office College, edited by R. W. Saunders and P. R. A. Brown, Reading, England, 1991.

Liou, K. N., Influence of cirrus clouds on weather and climate processes: A global perspective, *Mon. Weather Rev., 114*, 1167-1199, 1986.

Liou, K. N., *Radiation and Cloud Processs in the Atmosphere*, 487 pp., Oxford Univ. Press, New York, 1992.

Liou, K. N., Q. Fu, and T. P. Ackerman, A simple formulation of the delta-four-stream approximation for radiative transfer parameterizations, *J. Atmos. Sci., 45*, 1940-1947, 1988.

Liou, K. N., S. C. Ou, and G. Koening, An investigation on the climate effect of contrail cirrus, in *Air Traffic and the Environment: Background, Tendencies, and Potential Global Atmospheric Effects*, edited by U. Schumann, pp. 154-169, Springer-verlag, New York, 1990.

Macke, A., Scattering of light by polyhedral ice crystals, *Appl. Opt., 32*, 2780-2788, 1993.

Macke, A., J. Muller, and E. Rasche, Single scattering properties of atmospheric crystals, *J. Atmos. Sci., 53*, 2813-2825, 1996.

Mitchell, D. L., and W. P. Arnott, A model predicting the evolution of ice particle size spectra and radiative properties of cirrus clouds, II, Dependence of absorption and extinction on ice crystal morphology, *J. Atmos. Sci., 51*, 817-832, 1994.

Mitchell, D. L., S. K. Chai, Y. Liu, A. J. Heymsfield, and Y. Dong, Modeling cirrus clouds, I, Treatment of bimodal size spectra and case study analysis, *J. Atmos. Sci., 53*, 2952-2966, 1996a.

Mitchell, D. L., A. Macke, and Y. Liu, Modeling cirrus clouds, II, Treatment of radiative properties, *J. Atmos. Sci., 53*, 2967-2987, 1996b.

Press, W. H., S. A. Teukolsky, W. T. Vetterling, and B. P. Flannery, *Numerical Recipes in FORTRAN: The Art of Scientific Computing*, 702 pp., Cambridge Univ. Press, New York, 1986.

Pruppacher, H. P., and J. D. Klett, *Microphysics of Clouds and Precipitation*, 714 pp., D. Reidel, Norwell, Mass., 1980.

Sassen, K., D. O'C. Starr, G. G. Mace, M. R. Poellot, S. H. Melfi, W. L. Eberhard, J. D. Spinhire, E. W. Eloranta, D. E. Hagen, and J. Hallett, The 5-6 December 1991 FIRE IFO II jet stream cirrus case study: Possible influences of volcanic aerosols, *J. Atmos. Sci., 52*, 97-123, 1995.

Stephens, G. L., S. Tsay, P. W. Stackhouse Jr., and P. J. Flatau, The relevance of the microphysical and radiative properties of cirrus clouds to climate and climate feedback, *J. Atmos. Sci., 47*, 1742-1753, 1990.

Takano, Y., and K. N. Liou, Solar radiative transfer in cirrus clouds, I, single-scattering and optical properties of hexagonal ice crystals, J. *Atmos. Sci., 46*, 3-19, 1989a.

Takano, Y., and K. N. Liou, Solar radiative transfer in cirrus clouds, II, Theory and computation of multiple scattering in an anisotropic medium, *J. Atmos. Sci., 46*, 20-36, 1989b.

Takano, Y., and K. N. Liou, Radiative transfer in cirrus clouds, III, Light scattering by irregular ice crystals, *J. Atmos. Sci., 52*, 818-837, 1995.

van de Hulst, H. C., *Light Scattering by Small Particles*, 470 pp., Dover, Mineola, N.Y., 1957.

van de Hulst, H. C., *Multiple Light Scattering*, 739 pp., Academic, San Diego, Calif., 1980.

Warren, S. G., Optical constants of ice from the ultraviolet to the microwave, *Appl. Opt.*, *23*, 1206-1225, 1984.

Wylie, D. P., W. P. Menzel, H. M. Woolf, and K. L. Strabal, Four years of global cirrus clouds statistics using HIRS, *J. Climate*, *7*, 1972-1986, 1994.

Wyser, K., and P. Yang, Average ice crystal size and bulk single-scattering properties of cirrus clouds, *Atmos. Res.*, *49*, 315-335, 1998.

Yang, P., and K. N. Liou, Finite-difference time-domain method for light scattering by small ice crystals in three dimensional space, *J. Opt. Soc. Am. A Opt. Image Sci.*, *13*, 2072-2085, 1996a.

Yang, P., and K. N. Liou, Geometric-optics-integral-equation method for light scattering by nonspherical ice crystals, *Appl. Opt.*, *35*, 6568-6584. 1996b.

Yang, P., and K. N. Liou, Light scattering by hexagonal ice crystals: Solution by a ray-by-ray integration algorithm, *J. Opt. Soc. Am. A Opt. Image Sci.*, *14*, 2278-2288, 1997.

Yang, P., and K. N. Liou, Single-scattering properties of complex ice crystals in terrestrial atmosphere, *Contrib. Atmos. Phys.*, *71*, 223-248, 1998.

K. N. Liou and P. Yang, Department of Atmospheric Sciences, 7127 Math Sciences Building, University of California, Los Angeles, Los Angeles, CA 90095. (knliou@cloud.atmos.Ucla.EDU; yang@halo.atmos.Ucla.EDU)

D. Mitchell, Atmospheric Sciences Center, Desert Research Institute, Reno, NV 89506. (mitch@dri.edu)

K. Wyser, Department of Meteorology, Stockholm University, 106 91 Stockholm, Sweden. (klaus@misu.su.se)

(Received September 17, 1998; revised June 28, 1999; accepted July 8, 1999.)